INVESTIGATION OF THE EFFECT OF UNIAXIAL STRESS ON THE ELASTIC PROPERTIES OF $Rb_4LiH_3(SO_4)_4$

MOHAMMAD MAHBUBUR RAHMAN

Investigation of the Effect of Uniaxial Stress on the Elastic Properties of $Rb_4LiH_3(SO_4)_4$

by

© Mohammad Mahbubur Rahman

A thesis submitted to the
School of Graduate Studies
in partial fulfillment of the
requirements for the degree of
Master of Science.

Department of Physics & Physical Oceanography
Memorial University of Newfoundland

September 28, 2009

ST. JOHN'S NEWFOUNDLAND

Contents

Abstract

In this project, ultrasonic measurements have been used in order to observe the influence of uniaxial stress on the elastic properties of the ferroelastic compound $Rb_4LiH_3(SO_4)_4$. The experimental results are compared to predictions derived from a Landau model. In the experiment, uniaxial stresses either along [100] or [010] direction have been applied using two piezo-actuators mounted on opposite faces of the crystal. The temperature and pressure ranges for this investigation are 100 - 150K and 0 - 0.27 kbar, respectively. Throughout the investigation, it has been observed that in the absence of stress, the sound velocity along the x and z-axes shows a distinct step-like variation in the vicinity of the transition temperature, $T_c = 134$ K. The amplitude of the step-like variation is found to decrease with the application of a uniaxial stress. We believe that this is principally due to a reconfiguration of the domain distribution into the ferroelastic phase. This is supported by our Landau model which predicts no large variation over this pressure range.

Acknowledgements

It gives me immense pleasure to record the deepest sense of sincere gratitude to my supervisor Professor Dr. Guy Quirion, Department of Physics and Physical Oceanography, Memorial University, St. John's, NL, Canada for his continuous guidance, fruitful suggestions and invaluable comments during the entire period of my research work. It was a nice time for me at Memorial to carry out the research work under his knowledge and experience. I gratefully acknowledge Professor Dr. Maynard Clouter for giving permission to use his lab facility to prepare samples. I am very much indebted to Professor Dr. John K. C. Lewis for his nice teaching and assistance during the entire period of my study at Memorial. I would like to thank Dr. Kristin Poduska for her great teaching. I would like to thank Dr. Anand Yethiraj and Dr. J. Lagowski for their teaching. My special thanks to Fred Perry for his kind support in different times with computer related stuff. I would like to thank Gordon Whelan for making the probe for the pressure dependence ultrasonic measurements. My thanks go to Wayne Holly and Roger Guest for their kind service in supplying cryogens during my experimental work. A very special thank to Xuemei Han, my lab mate for her assistance in programming with Mathematica. I am also thanking Oktay Aktas, another of my lab mate for sharing different things in the lab during my work. I would like to express my thanks to Md. Nasir Uddin and other graduate students of Physics at Memorial and all my friends for their assistance regarding different matters during

the entire period of my study at Memorial.

I am immensely grateful to my family members back home for their love, patience, sacrifice and supports in various ways during the whole period of my stay in Canada. I am dedicating this thesis to my heavenly mother. Finally, all the thanks to the almighty, the most merciful and controller of the universe, whose commands make all the above mentioned facilities available to me.

Dedication

I would like to dedicate my thesis to the memory of the departed soul of my heavenly mom Mrs. Rabya Khatun, whose blessings enabled me to complete this noble work.

List of Tables

List of Figures

Chapter 1

Introduction

1.1 Introduction1

Over the past decades a large number of publications have been realized on single crystals with the chemical formula $A_4LiH_3(BO_4)_4$, where A= Rb, K, NH_4 and BO_4 = SO_4, SeO_4 [1, 2, 3, 4, 5, 6, 8]. Among this family of compounds, the best known ferroelastic is $Rb_4LiH_3(SO_4)_4$ [2, 4, 6, 8], hereafter abbrebiated as RLHS. This compound, which has a tetragonal symmetry (group 4) at room temperature, undergoes a structural phase transition at 134 K. The symmetry at low temperatures has been identified and it belongs to the monoclinic group 2. A crystal is said to be ferroelastic if structural domains are observed at low temperatures. The ferroelastic character of RLHS has been reported by the direct observation of a 90° domain structure [5]. The domain walls, observed in the plane (001), make an angle of 45° with the a and b axes parallel to the natural crystal edges [5]. The wall orientation in a ferroelastic phase is consistent with a 4→2 ferroelastic phase transition. The ferroelastic phase transition in RLHS has been also confirmed by optical, pyroelctric studies [5, 9], Brillouin scattering [7], and ultrasonic measurements [10]. According to the Brillouin scattering [7]

measurements, it has been reported that RLHS undergoes a second-order ferroelastic phase transition of 4→2 type at approximately $T_c = 115$ K. In their study, it was considered that the order parameter has two components, primary order parameter $(e_1 - e_2)$ and secondary order parameter e_6, where e_1, e_2 and e_6 are the spontaneous strains associated with a $4 \rightarrow 2$ transition (using Voigt notation). They also obtained that the effective elastic constant $\frac{1}{2}(C_{11} - C_{12})$, associated with the primary component of the order parameter, shows incomplete softening while the elastic constant C_{66} associated with the secondary order parameter exhibits very little temperature dependence.

Over the years, there has been some controversy regarding the true nature of the ferroelastic transition in RLHS. The investigation of the elastic properties, using ultrasonic technique [9, 10], Brillouin scattering technique [8, 11], and the series impedence method [4] have reported that the spontaneous strain is the order parameter, which means that the transition in RLHS is essentially proper ferroleastic. Study of Mróz et al. [7] also reported that the phase transition is governed by the combination of the strains $e_s = \alpha_1 (e_1 - e_2) + \alpha_6 e_6$. However, the detailed ultrasonic study of Quirion et al. [12] as a function of temperature and pressure rather indicates that the phase transition should be regarded as pseudoproper. The observed pressure and temperature dependence of the elastic constants has been found to agree well with predictions obtained from a pseudoproper ferroelastic Landau model. Throughout their work Quirion et al. [12] also proposed that a Raman B mode could be the primary order parameter. More recently, the pseudoproper character of the phase transition has been comfirmed by Raman scattering measurements [13] which clearly show that the order parameter is indeed associated with a B symmetry soft optic mode. Details about the proper and pseudoproper ferroelastic phase transition is given in Chapter 2 of section 2.3 and in Conclusion of the thesis as well.

Detailed analysis of the temperature and pressure dependence of the elastic properties of RLHS has been reported using ultrasonic measurements [12, 14]. Results obtained by their experimental work have been compared with the predictions of two phenomenological Landau models associated with a $4 \rightarrow 2$ ferroelastic transition. Within the framework of their analysis it has been reported that the proposed pseudoproper Landau model shows a good agreement with the temperature and pressure dependence of the elastic constants of RLHS in tetragonal phase. This fact has been put forward as a strong argument for the validity the proposed model. However, the quantitative agreement between the experimental data and the numerical predictions is not so good in the monoclinic phase. As pointed out, this discrepancy at low temperatures might be due to the existence of two ferroelastic domains perpendicular to each other [4]. This is supported by ultrasonic measurements [14] which show that the temperature dependence of the velocity of sound waves propagating along x and y-directions are equivalent in the monoclinic phase, which reflects the fact that the distribution of both domains is roughly half and half. As domains exist in the ferroelastic phase of RLHS, the ultrasonic velocity measurements cannot be used to test the model.

To get accurate values of elastic constants in monoclinic phase, measurements on single domain sample are required. According to Wolejko et al. [4], the application of a normal stress along [100] or [010] directions could be used to obtain a monodomain sample below T_c. Thus, the objective of this work is to study the influence of a uniaxial pressure on the sound velocity of RLHS. These experimental data are also compared to analytical predictions derived using a pseudoproper Landau model. The models used for the analysis are an extension of the Landau model which accounts very well for the temperature dependence of the spontaneous strains [12], the temperature and pressure dependence of the elastic constants [12, 14], the temperature dependence of

the soft optic mode [13], and the pressure dependence of the transition temperature.

The thesis has been organized in the following way, the objectives of the present work and a review of some earlier work are presented in Chapter 1. Chapter 2 includes general descriptions and applications of the ferroelastic materials. The physical properties of RLHS single crystals are given in Chapter 3. Details about the elastic properties of crystals are given in Chapter 4. Experimental techniques regarding ultrasonic velocity measurements on RLHS single crystals are described in Chapter 5. Chapter 6 contains the general description of Landau theory. In Chapter 7 we present the Landau analysis of the pressure dependence of the elastic properties of RLHS. The sample preparation technique for the experimental measurements and the results and discussions of our investigations are presented in Chapter 8. The summary of the experimental results and analytical predictions is presented in Chapter 9.

Chapter 2

Ferroelastic Materials

2.1 Ferroic Materials

Generally, a crystal is defined as ferroic (ferromagnetic, ferroelectric, or ferroelastic) if it has two or more possible orientational states (OS) in the absence of an external field such as magnetic, electric field or an external mechanical stress. These orientational states can then be switched from one to another by external fields. Thus, the equivalent states in ferromagnetic, ferroelastic, and ferroelectric materials can be switched by applying a magnetic field, a mechanical stress, and an electric field, respectively.

For example, let us consider ferromagnetic materials. The characteristic of ferromagnetic materials is the ease with which their magnetisation can be modified. The source of their magnetism is due to the magnetic moment possessed by certain electrons, which is the same as that in paramagnetic materials. The significant difference between ferromagnetism and paramagnetism is that the magnetic moments are randomly oriented in a paramagnetic state. So, in the absence of an external field no magnetization is observed on a macroscopic scale [15]. On the other hand, in fer-

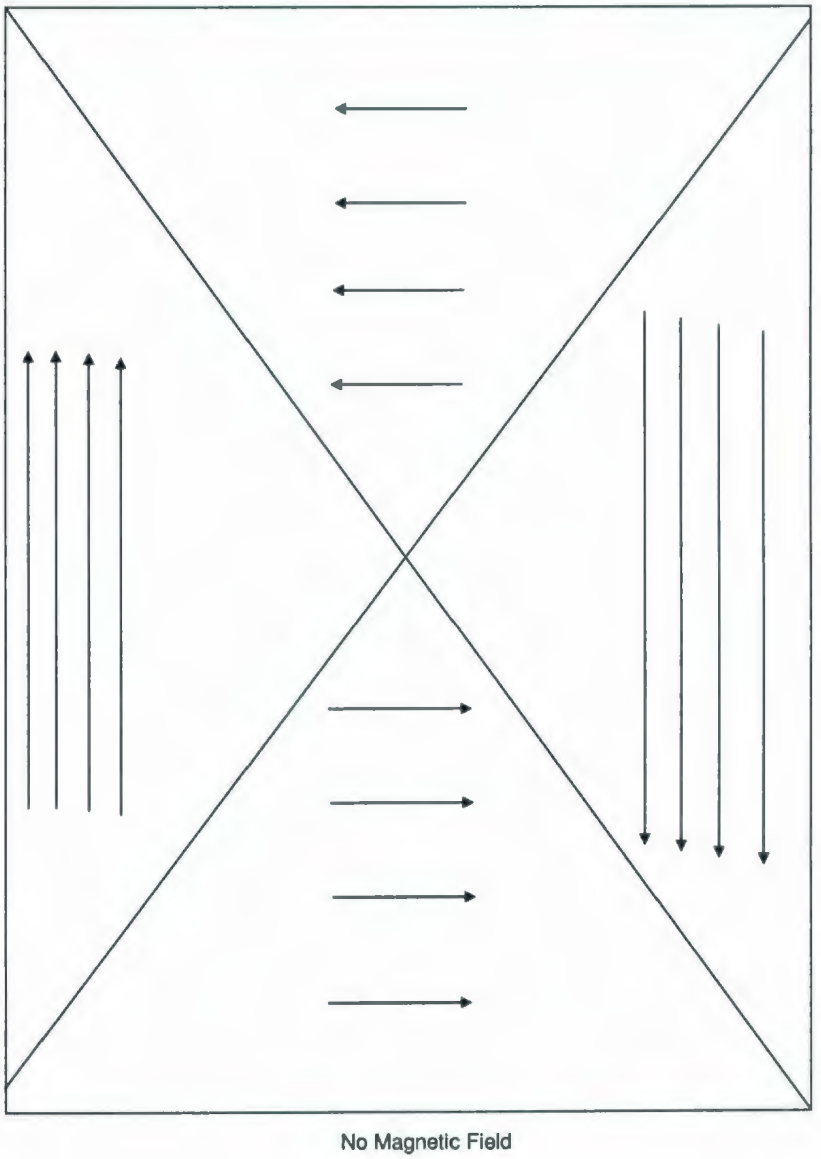

Figure 2.1: A possible ferromagnetic domain configuration in the absence of an external magnetic field. The arrows represent the magnetic moments.

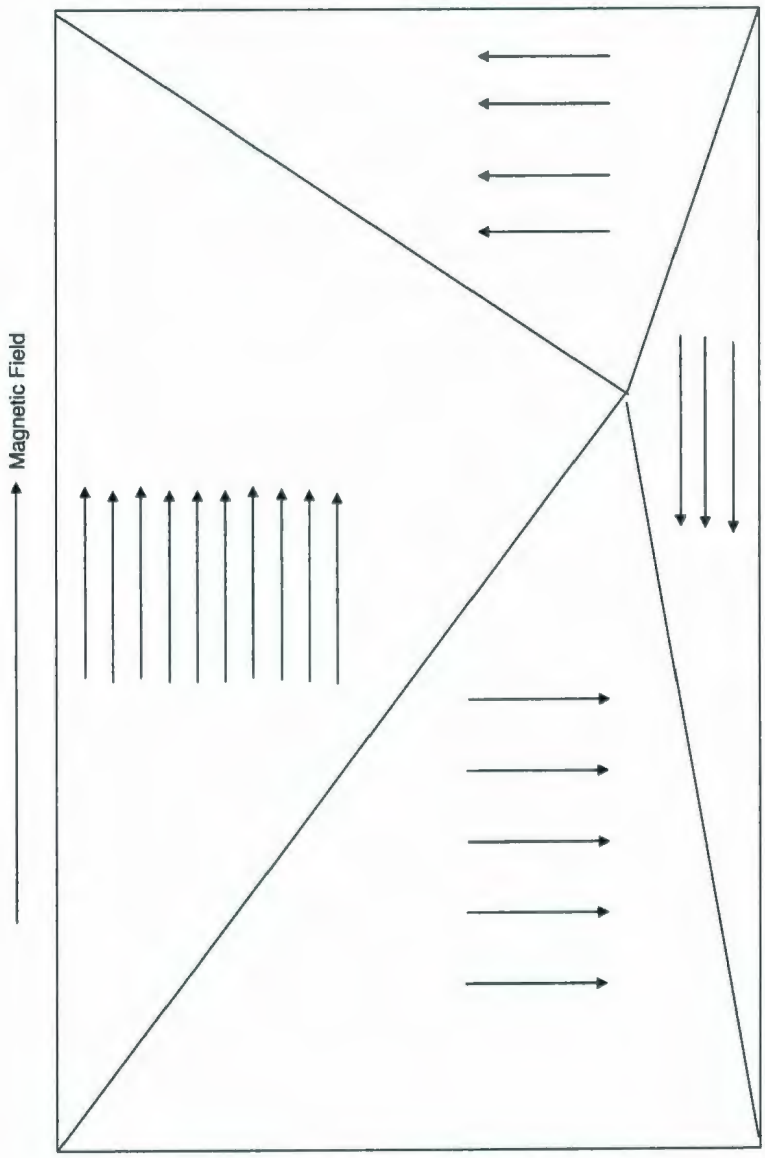

Figure 2.2: Ferromagnetic domains under the application of an external magnetic field.

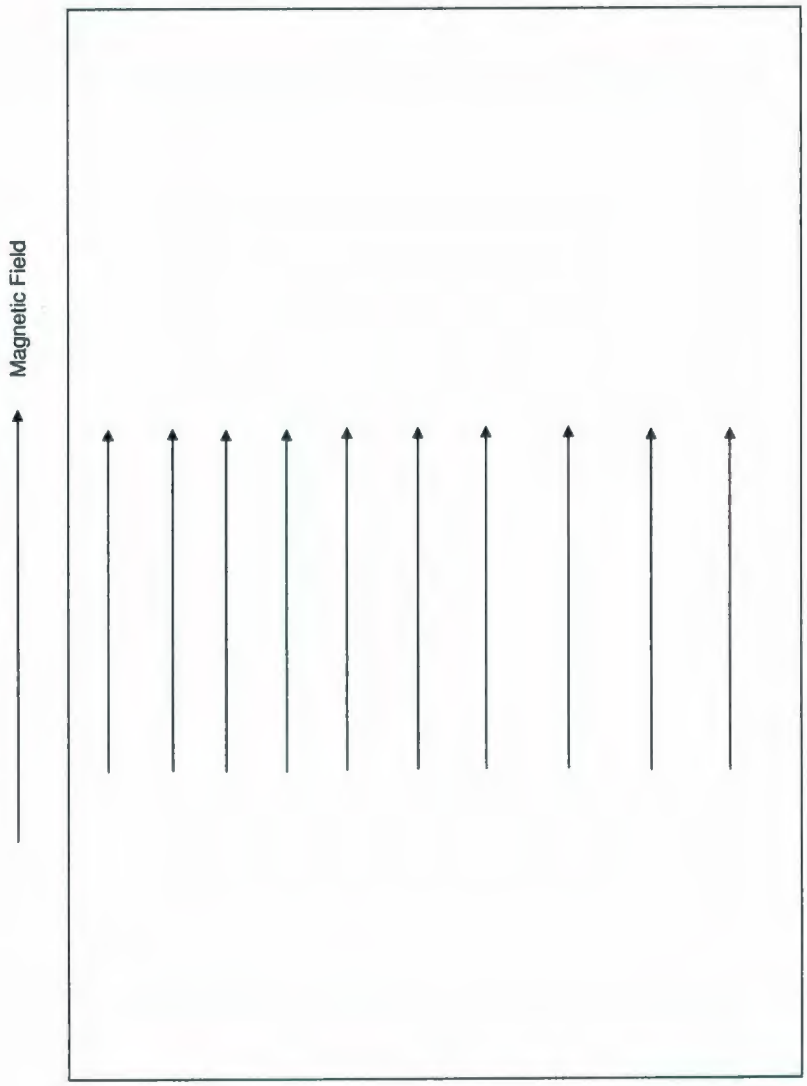

Figure 2.3: Under the action of a strong external magnetic field all the ferromagnetic domains are aligned along the field direction and the ferromagnetic material is converted to a monodomain state.

romagnetic substances, a remarkable degree of alignment is observed in the absence of any field. In 1907 Weiss [15] has given a satisfactory explanation by stating that there are forces between the elementary magnetic moments tending to make each one parallel to its neighbors. These forces cause the moments to be aligned in the same direction at absolute zero temperature. When the temperature is raised, deviation from perfect alignment increases until a critical temperature is reached, above that temperature the moments become randomly oriented, as in paramagnetic materials [15]. Thus, Weiss's theory successfully accounts for the fact that ferromagnetic materials are spontaneously magnetized even in the absence of an external magnetic field. However, the majority of the ferromagnetic materials are not strongly magnetized. In another theory Weiss overcome this difficulty by introducing the fact that the forces only maintained the parallel alignment over fairly small regions, called domains [15]. According to the Weiss hypothesis, a ferromagnetic material possesses a large number of domains with the magnetization held constant in magnitude and direction by the interactions within each domain, but varying in direction from one domain to the another. Domains are small regions in ferromagnetic substances within which all the magnetic moments are aligned parallel to each other [16]. Domains are usually too small to be observed by the naked eye [16]. At the domain boundaries the directions of the magnetic moments change and poles are formed at the surface of the material. Exchange energy of the electrons spin provides a strong driving force to align the magnetic moments parallel to each other and thus giving rise the formation of ferromagnetic domains. The formation of domains allows a ferromagnetic material to minimize its total energy [16].

Let us now discuss what happens to the ferromagnetic domains under the action of an external magnetic field. Fig. 2.1 represents the equilibrium state of a typical ferromagnetic material in the absence of an external magnetic field. When an exter-

nal magnetic field is applied, it results in a force which tends to align the moments along the direction of the applied field, moving the domain walls across the crystal [15]. The application of an external field rearranges the domains so as to increase the magnetization in the field direction. Eventually, as the strength of the field is increased, all domains align with the direction of the magnetic field (see Fig. 2.2). Whenever, the field becomes suffciently strong the material reaches the monodomain state characterized by a saturation in magnetization [15] (see Fig. 2.3). By analogy, the ferroelastic domains (stress domains) can by aligned by an external field corresponding to an external stress.

2.2 Applications of Ferroelastics

Ferroelastic materials have been extensively studied by different investigators [17, 18, 19] and they find application in the design of acoustic delay lines, modulators, transducers, shape memory devices, optical shutters, and superconducting squid devices. Another reason for the upsurge in research on ferroelasticity is that many natural minerals on our planet are ferroelastic materials and their interaction with biological activities, their corrosion, and geological behavior is largely determined by their ferroelastic or coelastic micro-structures [20, 21, 22]. Non-magnetic materials (ferroelastics and ferroelectrics) play an important role in a wide variety of technological applications. Some of the applications deal with dynamic domain processes such as electron emitters, thin-film memories while the others are concerned with the static distribution domains [23]. Research on ferroelastic materials has accelerated during the last decade for several other reasons [24]. Ferroelastics are potentially useful materials for nanotechnological applications, which is concerned with the production of man-made structures on a nano-meter length scale [24]. Hierarchal ferroelastic twin

patterns occur exactly on this length and ferroelastic crystal may hold the key for templating electronic nanostructures [24].

2.3 Ferroelastic Phase Transitions

The mechanism of ferroelastic phase transitions is understood better by comparing the phenomenological and microscopical models. Ferroelastic phase transitions are generally classified into two categories namely, proper ferroelastic transition, which considers order parameter as the spontaneous strains [5, 7, 9] and the pseudoproper ferroelastic phase transition in which the primary order parameter is generally an optical mode [7, 10, 25]. In pseudoproper ferroelastic phase transitions, a soft acoustic and a soft optical modes result from a coupling of the spontaneous strains with the actual order parameter. Thus, in pseudoproper ferroelastics, the spontaneous strain is a secondary order parameter while it is the primary order parameter for a proper ferroelastic phase transition [25].

If the proper ferroelastic phase transition is driven by a lattice-dynamical soft mode, the soft mode is a zone-centre ($k = 0$) acoustic phonon. Whenever an optical phonon softens, its frequency approaches zero. But at $k = 0$, the frequency of an acoustic mode is equal to zero as well. The difference between these two modes is that the softening of an optical mode means that its group velocity $\left(\frac{\partial\omega}{\partial k}\right)$ tends to zero at the transition [26, 27]. Most of the transitions in ferroelastic materials are pseudoproper in nature, rather than proper. In the former, the order parameter arises at the transition and has the same symmetry as the strain. In many cases, the order parameter is an optical soft mode and spontaneous strain arises because of its coupling with the order parameter. Now-a-days there are lots of different crystals showing pseudoproper ferroelastic phase transitions. Some important pseudoproper

crystals are LaP_5O_{14} [28, 29, 30], $BiVO_4$ [31, 32], $LaNbO_4$ [33], $Na_5Al_3F_{14}$ [32]. In these compounds ferroelastic softening of an optical phonon mode provides the order parameter and the spontaneous strain comes into play due to its bilinear coupling with the optical mode.

Chapter 3

Physical Properties of $Rb_4LiH_3(SO_4)_4$

3.1 Structure of $Rb_4LiH_3(SO_4)_4$ Single Crystals

The single crystals of $Rb_4LiH_3(SO_4)_4$ used in this investigation were grown at the crystal Physics Laboratory of Adam Mickiewicz University [7, 34] using an acid aqueous solution (P_H ¡ 1) containing stoichiometric amounts of Rb_2SO_4 and Li_2SO_4 at 310 K. Beakers containing the solution (5 ml) were tightly corked to slow down the evaporation rate at this temperature. The crystals obtained using this process are transparent, colorless, and show sharp optical extinction. For ultrasonic velocity measurements samples were cut in the form of cubes with 3 mm edges and opposite surfaces optically polished. The samples were placed in a holder which allowed the measurements of ultrasonic velocities in the temperature range from 100 to 300 K.

The chemical composition of RLHS was determined by atomic spectroscopy (Li^+, Rb^+) and chemical analysis ($SO_4{}^{-2}$) [10]. The structure consists of tetrahedral sulphate groups arranged together with Rb atoms on layers stacked perpendicularly to

the c-tetragonal axis. The four Rb atoms and SO_4 groups are distributed on two consecutive layers. The Li atoms are intercalated every two layers and are surrounded by tetrahedra of O atoms [35]. Morphological features of the synthesized crystals showed the tetragonal symmetry at room temperature. The crystals obtained were twinned and the twinning planes were found to be perpendicular to the tetragonal z-axis. The unit cell contains four layers of RLHS molecules, as shown in Fig. 3.1.

The composition of the single crystals of RLHS was confirmed by the preliminary powder x-ray diffraction (XRD) method as well as energy dispersive x-ray spectroscopy (EDAX) measurements [34]. A variable temperature powder XRD data [34] in the range 298 to 100 K confirmed the phase transition of RLHS. The diffraction intensities were measured with monochromatic molybdenum Ka radiation (λ= 0.7107 Å). The lattice parameters and detailed crystallographic data of RLHS determined by XRD [34] measurements are given in Table 3.1. In their study authors [34] have done the XRD measurements at temperatures 293 and 90 K respectively.

3.2 Ferroelastic Domains in $Rb_4LiH_3(SO_4)_4$

In ferroelastic materials, the various domain states have the same crystal structure but differ in their relative orientation. Thus, a domain state of a ferroelastic material is defined as a homogeneous portion of a given structure. Moreover, the domain wall orientation is closely related to the symmetry of the prototype phase. The orientations of domain walls can be found from crystallographic considerations such as symmetry of the prototype phase and symmetry of the ferroelastic phase.

Fig. 3.2 shows the 90° domain structure observed in the ferroelastic phase of RLHS at 110 K [5]. As reported in Ref. [5], the ferroelastic domain walls observed in the crystallographic plane (001) make an angle 45° with the natural crystal edges.

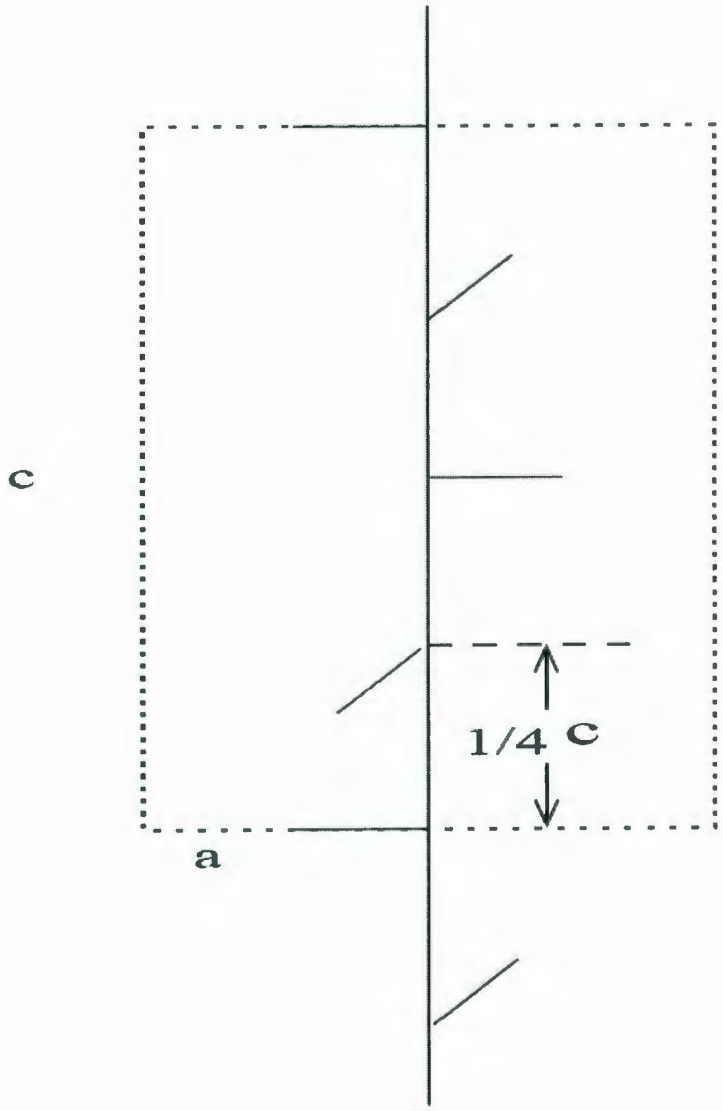

Figure 3.1: Symmetry of RLHS at room temperature. The horizontal bars represent the RLHS molecules while the vertical line representing the screw axes and the parallelogram indicates the unit cell of RLHS.

Table 3.1: Crystallographic data of RLHS measured by XRD technique [34].

Empirical formula	$Rb_4Li(HSO_4)_3(SO_4)$	$Rb_4Li(HSO_4)_3(SO_4)$
Crystal habit	Block	Block
Crystal color	Colorless	Colorless
Crystal system	Tetragonal	Monoclinic
Space group	$P4_3$	$P2_1$
Lattice parameters	$a = 7.629$ Å	$a = 7.583$ Å
—	$c = 29.497$ Å	$b = 29.230$ Å
—	—	$c = 7.536$ Å
Unit cell volume	1715.81 Å^3	1670.74 Å^3
Formula weight	736.1	736.1
Density	2.85 g/cm^3	2.93 g/cm^3

However, study of ferroelastic order parameter and domain walls in RLHS by Mróz et al. [36] indicates that the domain pattern consists of two mutually perpendicular walls rotated about z-axis by about 35° (see Fig. 3.3) away from the x-axis. Their study also reported that these walls do not rotate on cooling down to 100 K.

Ferroelastic domains exist due to the reduction in symmetry between the high and low temperature phases [37, 38]. The loss of symmetry elements in the tetragonal phase results in a very complicated domain structure in the monoclinic phase. Generally, domains form in ferroelastic materials to minimize the internal elastic energies. In the absence of external stress formation of domains in ferroelastic materials are entirely due to the generation of the strain during a co-elastic phase transition [39]. Their geometrical and physical properties follow the temperature evolution of the spontaneous strain. The shape of the domain walls is entirely dominated by the

elastic properties of the surrounding lattice and not by the local structural properties. By applying an appropriate stress the domain structure can be reoriented. In RLHS, as the domain walls lie in (001) plane making an angle 45° with the natural crystal edges, normal stress applied along [100] or [010] directions can be used to obtain a monodomain state [4, 5].

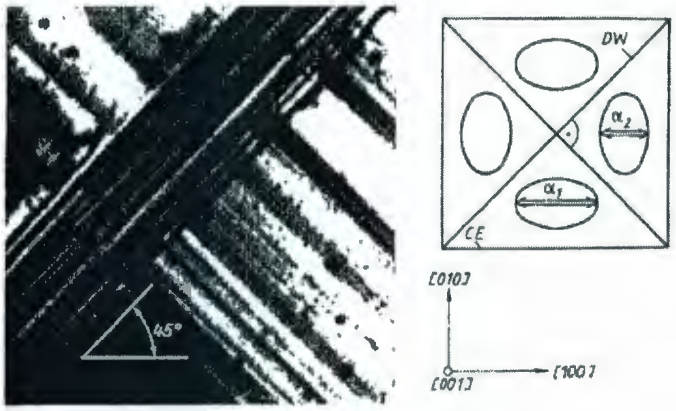

Figure 3.2: Ferroelastic domain structure observed in RLHS at 110 K. The orientation of the crystallographic axes are indicated with respect to the natural edges of the crystal. Here DW means the domain walls and CE stands for natural crystal edges. This picture is extracted from Ref. [5].

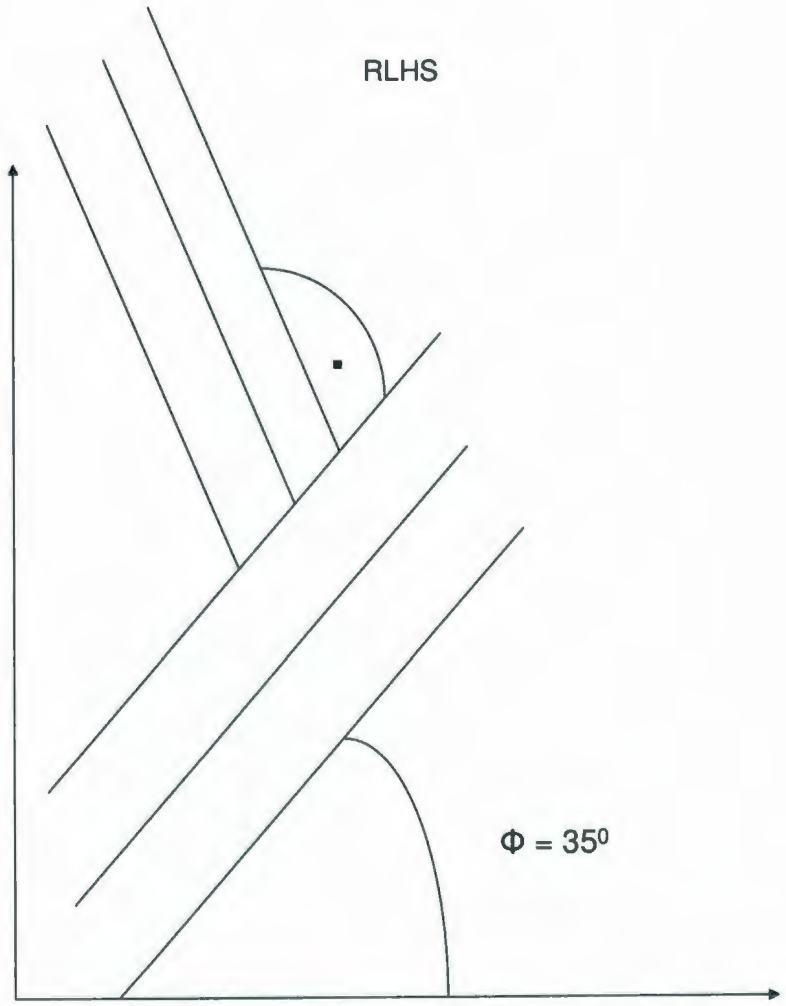

Figure 3.3: Schematic diagram of the W' domain wall orientation just below T_c. This picture is extracted from Ref. [36].

Chapter 4

Elastic Properties of Crystals

4.1 Deformations and Strain

A crystal is said to be deformed if the mean positions of its atoms are changed. The deformations could change the sample's shape and volume. In a homogeneous continuum, the position of any point can be defined by a vector $\mathbf{r}$ with components (x_1, x_2, x_3) relative to some reference frame [40]. Under the action of external forces, the crystal gets deformed and the position vector changes to $\mathbf{r}'$ with components (x'_1, x'_2, x'_3). Thus, the displacement is simply given by

$$u_i = x'_i - x_i \tag{4.1}$$

where u_i represents the components of the displacement vector.

As a result of deformation, the distance $\mathbf{dl}$ between two points is changed to $\mathbf{dl}'$. If we consider two very close points, separated by components dx_i along the direction i, after deformations $dx'_i = dx_i + du_i$. Adopting the Einstein notation, where repeated indices represent a sum over that index [40],

$$dl'^2 = dx'_i dx'_i = (dx_i + du_i)^2 . \tag{4.2}$$

For infinitesimal deformations, using that $du_i = \frac{\partial u_i}{\partial x_k} dx_k$, we obtain

$$dl'^2 = dl^2 + 2\frac{\partial u_i}{\partial x_k} dx_i dx_k + \frac{\partial u_i}{\partial x_k}\frac{\partial u_i}{\partial x_l} dx_k dx_l \ . \tag{4.3}$$

Interchanging the dummy suffices i with l, we can write

$$dl'^2 = dl^2 + 2e_{ik} dx_i dx_k \tag{4.4}$$

where the tensor elements e_{ik} are given by

$$e_{ik} = \frac{1}{2}\left(\frac{\partial u_i}{\partial x_k} + \frac{\partial u_k}{\partial x_i} + \frac{\partial u_l}{\partial x_i}\frac{\partial u_l}{\partial x_k}\right) \ . \tag{4.5}$$

As indicated by Eq. 4.5, the strain tensor associated with deformations is necessarily symmetric, i.e.,

$$e_{ik} = e_{ki} \ . \tag{4.6}$$

Thus, for small deformations, the strain tensor reduces to

$$e_{ik} = \frac{1}{2}\left(\frac{\partial u_i}{\partial x_k} + \frac{\partial u_k}{\partial x_i}\right) \ . \tag{4.7}$$

In the case of a three dimensional material the deformations introduced by external forces can be represented by a 3×3 strain tensor whose elements are given below

$$\mathrm{e} = \begin{bmatrix} e_{11} & e_{12} & e_{13} \\ e_{12} & e_{22} & e_{23} \\ e_{13} & e_{23} & e_{33} \end{bmatrix} \tag{4.8}$$

where i, j extends from 1 to 3. The diagonal elements represent the variations in length along the crystallographic axes, while the non-diagonal components define shear deformations. Considering the symmetry properties described in Eq. 4.6, the number of independent elements in the strain tensor is 6.

4.2 Stress

The stress is defined as the force acting per unit area in a material. The internal stresses arise due to the interaction between molecules in a crystal. We can assume that for any part of a substance the resultant internal stress is given by the following integral [40]

$$\int f_i dV \quad . \tag{4.9}$$

where f_i is the force acting on the volume element dV. According to the vector analysis, f_i must be the divergence of a tensor of rank two. Therefore the above integration can be expressed as [40]

$$\int \frac{\partial \sigma_{ik}}{\partial x_k} dV = \oint \sigma_{ik} da_k \tag{4.10}$$

where da_k are the force components acting on the surface element **da** and σ_{ik} is the stress tensor. Thus, σ_{ik} $\mathbf{da}_k$ is the i-th component of the force acting on the surface element of **da**. In the Cartesian coordinate system, the component σ_{ik} of the stress tensor is produced by the i-th component of a force acting on unit area normal to the x_k-axis. There are nine components of the stress tensor σ_{ik}, where $i, j = 1, 2, 3$. Like the strain tensor, the stress tensor is symmetric. Based on the following symmetry consideration the number of independent elements of the stress tensor is reduced to six [40],

$$\sigma_{ik} = \sigma_{ki} \quad . \tag{4.11}$$

4.3 Hooke's Law

A medium is said to be elastic if it returns back to its initial state after external forces are removed. This is due to the internal stress, which act to restore the system into its initial state. This simple principle is expressed by the Hooke's law which gives the

fundamental relationship between the applied force and the amount of deformations experienced by a material. If the deformations are sufficiently small, the induced stresses can be written as a Taylor series expansion

$$\sigma_{ij}\left(e_{kl}\right)=\sigma_{ij}\left(0\right)+\left(\frac{\partial\sigma_{ij}}{\partial e_{kl}}\right)_{e_{kl}=0}e_{kl}+\frac{1}{2}\left(\frac{\partial^{2}\sigma_{ij}}{\partial e_{kl}\partial e_{mn}}\right)_{e_{kl}=e_{mn}=0}e_{kl}e_{mn}+\ldots \quad (4.12)$$

As $\sigma_{ij}\left(0\right)=0$, the dominant term of Eq. 4.12 [41] reduces to

$$\sigma_{ij}=C_{ijkl}e_{kl} \quad (4.13)$$

where

$$C_{ijkl}=\left(\frac{\partial\sigma_{ij}}{\partial e_{kl}}\right)_{e_{kl}=0} . \quad (4.14)$$

Eq. 4.13 is the explicit form of the Hooke's law which states that within the elastic limit the strain is directly proportional to the applied stress. The coefficients C_{ijkl} represent elements of a fourth rank elastic stiffness tensor which describes the relationship between the stress and strain in the crystal. Since the tensors σ and e are both symmetric, the elastic constants defined by Eq. 4.14 must remain invariant under the permutation of i and j or k and l, i.e.,

$$C_{ijkl}=C_{jikl};\quad C_{ijkl}=C_{ijlk} . \quad (4.15)$$

The stress exerted on a material can also be expressed in terms of the variation in the internal energy with respect to the strain

$$\sigma_{ij}=\frac{\partial U}{\partial e_{ij}} . \quad (4.16)$$

Thus, the elastic constant C_{ijkl} defined in Eq. 4.14 can also be written as

$$C_{ijkl}=\frac{\partial^{2}U}{\partial e_{ij}\partial e_{kl}} . \quad (4.17)$$

4.4 Elastic Properties of Crystals

The Hooke's law, governing the relation between stress σ_{ij} and strain e_{kl}, is given by Eq. 4.13, where C_{ijkl} are the components of a fourth-rank tensor called elastic stiffness tensor. This elastic stiffness tensor C_{ijkl} has 81 entries. Since both the stress and strain tensors are symmetric, the number of independent elastic constants is reduced to 36. Taking advantage of symmetry properties, the independent elastic constants can be label using two indices. According to the Voight notation, the indices are written in the following way:

$$\begin{gathered}(11) \leftrightarrow 1, \quad (22) \leftrightarrow 2, \quad (33) \leftrightarrow 3 \\ (23) = (32) \leftrightarrow 4, \quad (31) = (13) \leftrightarrow 5, \quad (12) = (21) \leftrightarrow 6 \ .\end{gathered} \tag{4.18}$$

Therefore, the 36 independent elastic constants are represented by a 6×6 matrix, with

$$C_{\alpha\beta} = C_{ijkl} \tag{4.19}$$

where, $\alpha \leftrightarrow (ij)$, $\beta \leftrightarrow (kl)$ and $\alpha, \beta = 1, 2, 3, ..6$. This notation can also be used to represent the stress and strain tensors. In terms of Voight notation, Eq. 4.17 leads to the condition

$$C_{\alpha\beta} = C_{\beta\alpha} \tag{4.20}$$

reducing the number of independent elastic constants to a maximum of 21 [41].

$$\mathrm{C} = \begin{bmatrix} C_{11} & C_{12} & C_{13} & C_{14} & C_{15} & C_{16} \\ C_{12} & C_{22} & C_{23} & C_{24} & C_{25} & C_{26} \\ C_{13} & C_{23} & C_{33} & C_{34} & C_{35} & C_{36} \\ C_{14} & C_{24} & C_{34} & C_{44} & C_{45} & C_{46} \\ C_{15} & C_{25} & C_{35} & C_{45} & C_{55} & C_{56} \\ C_{16} & C_{26} & C_{36} & C_{46} & C_{56} & C_{66} \end{bmatrix} \tag{4.21}$$

This elastic constant tensor is used to represent the elastic properties of crystals with triclinic structure. In the case of crystals with higher symmetry, the number of independent elastic constants is reduced further by imposing symmetry constraints.

Under the application of the symmetry operations, as the crystal remains invariant, any tensors describing the properties of that crystal must also remain unchanged. Generally, the change of reference is defined by the coefficients $\alpha_i{}^k$ of the relations giving the new basis vectors x_1', x_2', x_3' in terms of the old ones x_1, x_2, x_3, according to

$$x_i' = \alpha_i^k x_k \quad . \tag{4.22}$$

Here $\alpha_i{}^k$ are elements of the transformation matrix associated with some symmetry operation. In matrix form Eq. 4.22 is given as

$$\begin{bmatrix} x_1' \\ x_2' \\ x_3' \end{bmatrix} = \begin{bmatrix} \alpha_1{}^1 & \alpha_1{}^2 & \alpha_1{}^3 \\ \alpha_2{}^1 & \alpha_2{}^2 & \alpha_2{}^3 \\ \alpha_3{}^1 & \alpha_3{}^2 & \alpha_3{}^3 \end{bmatrix} \begin{bmatrix} x_1 \\ x_2 \\ x_3 \end{bmatrix} \quad . \tag{4.23}$$

If we consider a second-rank tensor σ, the transformation rule can be written as

$$\sigma_{ij}{}' = \alpha_i{}^p \alpha_j{}^q \sigma_{pq} \quad . \tag{4.24}$$

Likewise, for the elastic stiffness tensor, the element C_{pqrs} (a fourth-rank tensor) transforms as

$$C_{ijkl} = \alpha_i{}^p \alpha_j{}^q \alpha_k{}^r \alpha_l{}^s C_{pqrs} \; . \tag{4.25}$$

If the transformation corresponds to a symmetry operation, the invariance condition requires that

$$C_{ijkl} = C_{pqrs} \tag{4.26}$$

i.e.,

$$C_{ijkl} = \alpha_i{}^p \alpha_j{}^q \alpha_k{}^r \alpha_l{}^s C_{ijkl} \quad . \tag{4.27}$$

This states that elastic constants are non zero only if ${\alpha_i}^i {\alpha_j}^j {\alpha_k}^k {\alpha_l}^l = 1$. Comparing to the triclinic crystals, the low symmetry monoclinic phase of point group 2 possesses an additional symmetry. That is, RLHS is invariant under a 180^0 rotation around the z-axis. In this case, the α-matrix is defined as

$$\alpha = \pm \begin{bmatrix} -1 & 0 & 0 \\ 0 & -1 & 0 \\ 0 & 0 & 1 \end{bmatrix} \tag{4.28}$$

This states that all coefficients with an odd number of index 3 (for which ${\alpha_i}^i {\alpha_j}^j {\alpha_k}^k {\alpha_l}^l = -1$) must vanish. Therefore, for a monoclinic structure the number of independent elastic constants reduces to 13,

$$\mathrm{C}_{mono} = \begin{bmatrix} C_{11} & C_{12} & C_{13} & 0 & 0 & C_{16} \\ C_{12} & C_{22} & C_{23} & 0 & 0 & C_{26} \\ C_{13} & C_{23} & C_{33} & 0 & 0 & C_{36} \\ 0 & 0 & 0 & C_{44} & C_{45} & 0 \\ 0 & 0 & 0 & C_{45} & C_{55} & 0 \\ C_{16} & C_{26} & C_{36} & 0 & 0 & C_{66} \end{bmatrix}. \tag{4.29}$$

In the high symmetry phase, RLHS belongs to the tetragonal point group 4 [42]. Thus, the elastic tensor must be invariant relative to a 90^0 rotation about the Z-axis. Under the symmetry operation ${C_4}^1$, the coordinates transform as

$$X \text{ chnages to } Y;$$
$$Y \text{ changes to } -X \text{ and}$$
$$Z \text{ remains as } Z$$

Therefore, the elastic constants transforms as

$$C_{22} = C_{2222} \rightarrow C_{1111} = C_{11} \tag{4.30}$$

$$C_{23} = C_{2233} \rightarrow C_{1133} = C_{13} \tag{4.31}$$

$$C_{55} = C_{1313} \rightarrow C_{2323} = C_{44} \tag{4.32}$$

$$C_{26} = C_{2212} \rightarrow -C_{1121} = -C_{16} \tag{4.33}$$

$$C_{36} = C_{3312} \rightarrow -C_{3312} = -C_{36} = 0 \tag{4.34}$$

Thus, in the high symmetry (tetragonal) phase the total number of independent elastic constants reduces to 7 and the corresponding tensor is

$$\mathrm{C}_{tetra} = \begin{bmatrix} C_{11} & C_{12} & C_{13} & 0 & 0 & C_{16} \\ C_{12} & C_{11} & C_{13} & 0 & 0 & -C_{16} \\ C_{13} & C_{13} & C_{33} & 0 & 0 & 0 \\ 0 & 0 & 0 & C_{44} & 0 & 0 \\ 0 & 0 & 0 & 0 & C_{44} & 0 \\ C_{16} & -C_{16} & 0 & 0 & 0 & C_{66} \end{bmatrix} . \tag{4.35}$$

4.5 Elastic Energy

A crystal gains elastic energy if the atoms equilibrium positions are changed by the application of external stress. In the case of small deformations, elastic energy is expressed as

$$F_{el} = \frac{1}{2} C_{\alpha\beta} e_\alpha e_\beta \tag{4.36}$$

where $\mathrm{C}_{\alpha\beta}$ are elements of the elastic stiffness tensor expressed in terms of the Voigt notation with α and β ranging from 1 to 6. This elastic potential energy F_{el} is the change in internal energy of the material per unit volume. With the help of Eq. 4.36, the elastic energy of RLHS in the paraelastic (tetragonal) phase is given by,

$$\begin{aligned} F_{el} = &\frac{1}{2} C_{11}({e_1}^2 + {e_2}^2) + \frac{1}{2} C_{44}({e_4}^2 + {e_5}^2) + \frac{1}{2} C_{33} {e_3}^2 \\ &+ \frac{1}{2} C_{66} {e_6}^2 + C_{12} e_1 e_2 + C_{13}(e_1 + e_2) e_3 + C_{16}(e_1 - e_2) e_6 \, . \end{aligned} \tag{4.37}$$

4.6 Propagation of Elastic Waves in Crystals

In general, for anisotropic media three different kinds of waves can propagate in a given direction. In principle, for a given direction, one observes the following three waves: a quasi-longitudinal wave, a fast quasi-transverse wave and a slow quasi-transverse wave. These three waves have different velocities and their polarizations are always mutually orthogonal.

In order to obtain the equations of motion in an elastic medium [41, 40] we must solve Newton's second law of motion,

$$\rho \frac{\partial^2 u_i}{\partial^2 t} = \frac{\partial \sigma_{ik}}{\partial x_k} \quad . \tag{4.38}$$

Inserting the Hooke's law stated in Eq. 4.13 in Eq. 4.38, we obtain

$$\rho \frac{\partial^2 u_i}{\partial^2 t} = C_{ijkl} \frac{\partial^2 u_l}{\partial x_j \partial x_k} \quad . \tag{4.39}$$

If we consider a monochromatic elastic wave of frequency ω propagating along the direction given by the wave vector k, we might seek for plane wave type solutions of the form,

$$u_i = u_{0i} e^{i(\mathbf{k}.\mathbf{r}-\omega t)}, i = 1, 2, 3 \tag{4.40}$$

where u_{0i} represents the atomic displacement amplitude along the i-direction. That direction also corresponds to the wave polarization vector. Inserting Eq. 4.40 into Eq. 4.39 and putting $u_{0i} = \delta_{il} u_{0l}$, we find

$$\left(\rho\omega^2 \delta_{il} - C_{ijkl} k_j k_k\right) u_{ol} = 0 \quad . \tag{4.41}$$

Dividing Eq. 4.41 by k^2, we get

$$\left(\rho v^2 \delta_{il} - C_{ijkl} n_j n_k\right) u_{ol} = 0 \quad . \tag{4.42}$$

This is a set of three homogeneous equations of the first degree for the unknowns u_x, u_y, u_z. The above equation is the well-known Christoffel equation, where $v = \frac{\omega}{k}$ represents the phase velocity of the acoustic wave. Here, n_j, n_k are the cosine direction of the **k** with respect to the axes of x, y, and z, respectively. Such equations have non-zero solutions only if the determinant

$$\left|\Gamma_{il} - \rho v^2 \delta_{il}\right| = 0 \tag{4.43}$$

with

$$\Gamma_{il} = C_{ijkl} n_j n_k \tag{4.44}$$

where Γ_{il} is a second-rank tensor. Eq. 4.43 is the well-known secular equation, which gives solutions for the velocities. The propagation tensor, Γ has the eigenvalue ρv^2. Since Γ_{il} contains the elastic constants, the wave velocities are thus related to the independent elastic constants of the crystal. Generally, there are three possible relations between ω and **k** for any direction in the crystal and hence there will be three different velocities corresponding to the three elastic waves. If we consider the propagation tensor Γ along z-direction ($n_1 = n_2 = 0$, $n_3 = 1$) then Γ_{il} can be written as Γ_{il}=C_{i33l}, or, explicitly as

$$\Gamma = \begin{bmatrix} C_{55} & C_{45} & C_{35} \\ C_{45} & C_{44} & C_{34} \\ C_{35} & C_{34} & C_{33} \end{bmatrix} . \tag{4.45}$$

In the high symmetry (tetragonal) phase of RLHS, we know that C_{35}=C_{34}=C_{45}=0 and that C_{44}=C_{55}. Therefore, for waves propagating along the z -direction, the propagation tensor Γ now becomes

$$\Gamma = \begin{bmatrix} C_{44} & 0 & 0 \\ 0 & C_{44} & 0 \\ 0 & 0 & C_{33} \end{bmatrix} \tag{4.46}$$

The eigenvalues of Γ are given by $\lambda_1 = C_{33}$ and $\lambda_2 = \lambda_3 = C_{44}$, where $\lambda_1 = \lambda_2 = \lambda_3 = \rho v^2$. Therefore, the velocities for the three waves propagating along the z-direction direction can be calculated in terms of the elastic constants as

$$v_1 = \sqrt{\left(\frac{C_{33}}{\rho}\right)}, v_2 = v_3 = \sqrt{\left(\frac{C_{44}}{\rho}\right)} \quad . \tag{4.47}$$

The corresponding eigenvectors are

$$u_1 = (0,0,1)\,, u_2 = (0,1,0)\,, u_3 = (1,0,0) \tag{4.48}$$

All the eigenvectors are normalized which are representing the polarizations of the corresponding waves. The polarization of the first wave is parallel to the z-direction and therefore belongs to the longitudinal mode, whereas the polarizations of the other two waves are perpendicular to the first wave and consequently belong to transverse modes. Likewise, the velocities and modes of the sound waves propagating along [100], [010] and [110] for both the low symmetry (monoclinic) phase and high symmetry (tetragonal) phase of RLHS can be calculated. The results of the calculations are presented in Table 4.1. Here L and T are used to represent longitudinal and transverse modes respectively. The subscripts represent the direction of polarization for a direction of propagation given in the square bracket.

Table 4.1: Expressions of ρv^2 as a function of elastic constants in high symmetry (tetragonal) and low symmetry (monoclinic) phases, where L and T_i stand for the longitudinal and transverse wave polarized along i-direction respectively.

Direction	Mode	High Symmetry Phase	Low Symmetry Phase
[100]	L	$\frac{1}{2}\left(C_{11}+C_{66}+\sqrt{(C_{11}-C_{66})^2+4C_{16}^2}\right)$	$\frac{1}{2}\left(C_{11}+C_{66}+\sqrt{(C_{11}-C_{66})^2+4C_{16}^2}\right)$
-	T_y	$\frac{1}{2}\left(C_{11}+C_{66}-\sqrt{(C_{11}-C_{66})^2+4C_{16}^2}\right)$	$\frac{1}{2}\left(C_{11}+C_{66}-\sqrt{(C_{11}-C_{66})^2+4C_{16}^2}\right)$
-	T_z	C_{44}	C_{55}
[010]	L	$\frac{1}{2}\left(C_{11}+C_{66}+\sqrt{(C_{11}-C_{66})^2+4C_{16}^2}\right)$	$\frac{1}{2}\left(C_{22}+C_{66}-\sqrt{(C_{22}-C_{66})^2+4C_{26}^2}\right)$
-	T_x	$\frac{1}{2}\left(C_{11}+C_{66}-\sqrt{(C_{11}-C_{66})^2+4C_{16}^2}\right)$	$\frac{1}{2}\left(C_{22}+C_{66}+\sqrt{(C_{22}-C_{66})^2+4C_{26}^2}\right)$
-	T_z	C_{44}	C_{44}
[001]	L	C_{33}	C_{33}
-	T_x	C_{44}	$\frac{1}{2}\left(C_{44}+C_{55}+\sqrt{(C_{44}-C_{55})^2+4C_{45}^2}\right)$
-	T_y	C_{44}	$\frac{1}{2}\left(C_{44}+C_{55}-\sqrt{(C_{44}-C_{55})^2+4C_{45}^2}\right)$
[110]	L	$\frac{1}{2}\left(C_{11}+C_{66}+\sqrt{(C_{12}+C_{66})^2+4C_{16}^2}\right)$	...
-	$T_{[110]}$	$\frac{1}{2}\left(C_{11}+C_{66}-\sqrt{(C_{12}+C_{66})^2+4C_{16}^2}\right)$	...
-	T_z	C_{44}	$\frac{1}{2}(C_{44}+2C_{45}+C_{55})$

Chapter 5

Experimental Techniques

The goal of this project is to investigate the effect of uniaxial stress on the elastic properties of RLHS single crystals and to compare the experimental results to analytical predictions obtained using a Landau model. For that purpose a high-resolution acoustic interferometer device has been used for ultrasonic velocity measurements as a function of temperature on single crystal under uniaxial pressure. In this chapter we describe how the ultrasonic velocity can be measured using the standard pulse echo method. For high resolution measurements this technique is used in conjunction with an acoustic interferometer also presented in this chapter.

5.1 Sound Velocity Measurements

Usually, ultrasonic velocity measurement is done at a maximum frequency of 10 MHz. However, in many applications of ultrasonics a very high frequency up to 5 GHz range is used as well. In our measurement, the sound velocity measurement is done with a standard pulse-echo method with a frequency around 30 MHz. The schematic diagram is shown in Fig. 5.1. A transducer, consisting of a small piezoelectric crystal and two

electrodes, is mounted on the top surface of the sample. An rf signal is applied to the electrodes of the transducer it order to generate mechanical vibrations. Due to the piezoelectric effect, the transducer vibrates with the same frequency as that of the oscillating applied field. The generated mechanical vibrations produce a sound wave which propagates back and forth between the extremities of the crystal. Each time the sound wave returns back to the transducer, a small fraction of the mechanical energy is converted into electrical signal (inverse piezo-electric effect). As the sound wave propagates back and forth between the extremities of the crystal, due to reflection at the boundaries, a multi-echo pattern can be observed on an oscilloscope. In the reflection configuration, the absolute sound velocity can be determined using the following relation

$$v = \frac{2L}{\Delta t} \tag{5.1}$$

where L is the sample's length while Δt corresponds to the time of flight for one round trip. If the uncertainties are taken into account, the typical uncertainty in the absolute velocity measurement is a few percent. For that reason, the standard pulse-method is not always sensitive enough to detect variations at a phase transition. To achieve higher resolution, an acoustic interferometer device can be used.

5.2 Acoustic Interferometer

The acoustic interferometer device measures the relative change in velocity $\frac{\Delta v}{v}$ instead of the absolute velocity. The basic idea of this method is to measure the phase difference between a reference signal generated by a synthesizer with that of an echo signal coming out of the sample. The schematic of the interferometer is illustrated in Fig. 5.2. As shown in the diagram, a continuous rf signal is produced by a synthesizer (6061A Synthesized RF Generator). This rf signal is divided into two parts by the

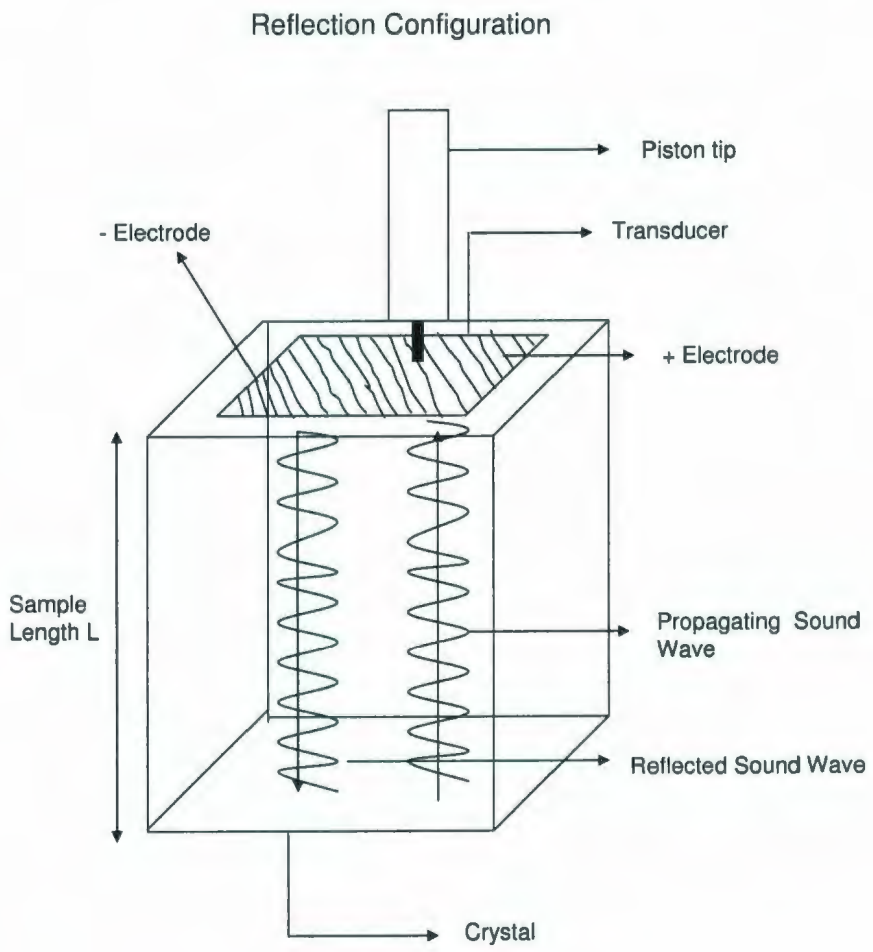

Figure 5.1: Schematic diagram of the propagation of sound waves through RLHS in the reflection configuration.

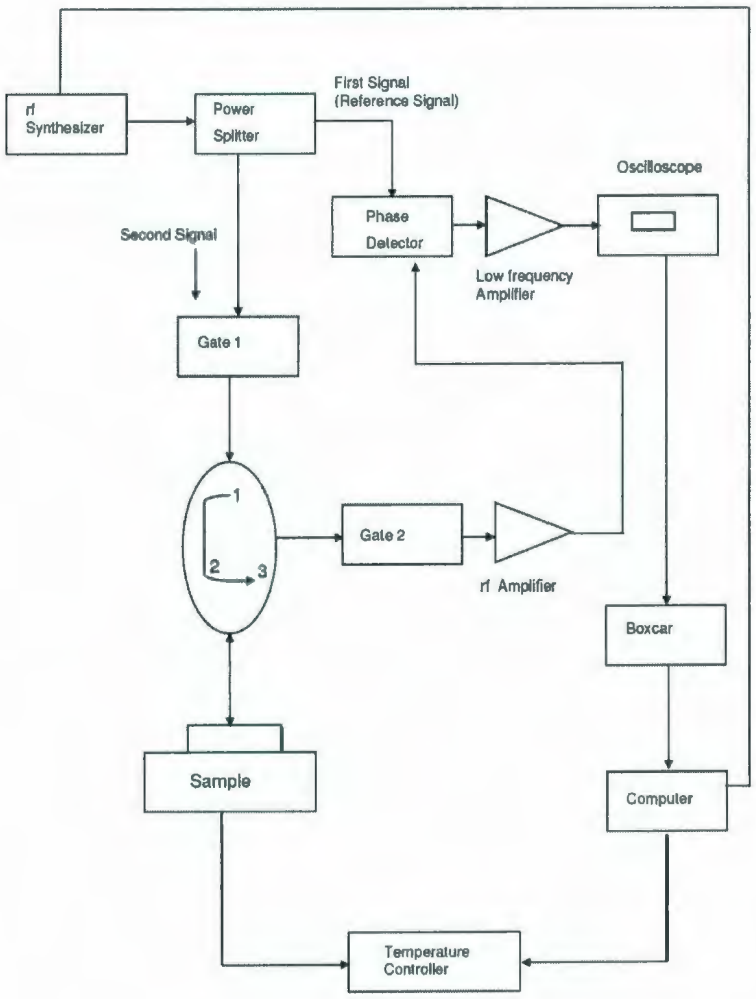

Figure 5.2: Schematic diagram of the acoustic interferometer device.

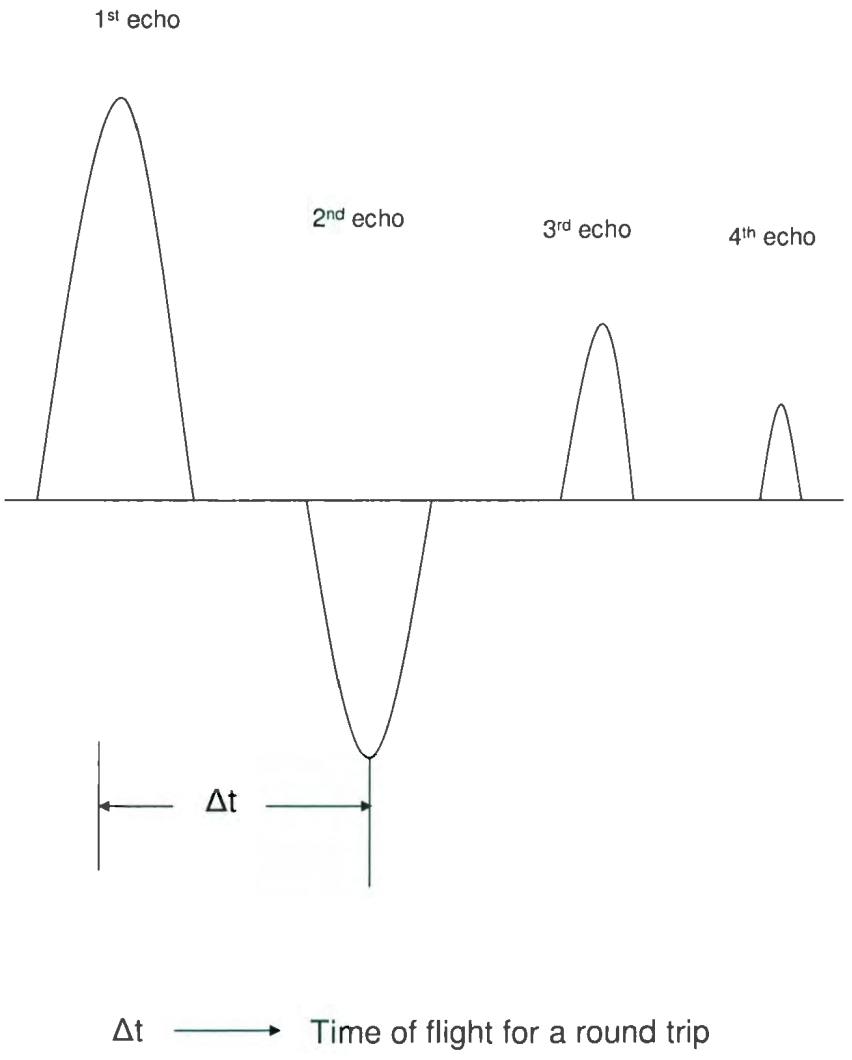

Figure 5.3: A typical multi-echo system observed on the oscilloscope.

power splitter. The first portion of the signal is used as the reference, while the second portion is sent to gate 1 which generates a series of short pulses (smaller than μs) at a rate of about 1 kHz. As the rf pulse reaches the transducer, the signal is converted into an acoustic wave which propagates through the sample. This acoustic wave travels between the extremities of the sample. Each time the wave reaches the transducer, a small fraction of the acoustic energy is converted back into a rf signal. The multi-echo pattern enters the circulator at position 2 and comes out at position 3. To prevent saturation of the low noise rf amplifier, a gate (gate 2) is used to cut off the initial pulse from the echo pattern. A phase comparator is then used to measure the phase difference between the reference signal and the reflected signal. A typical multi-echo pattern observed on an oscilloscope is shown in Fig. 5.3. During the experiment, a boxcar is used to measure the phase of one of specific echo. For the n^{th} echo, considering that the time of flight is $\Delta t_n = \frac{2nL}{v}$ for a rf signal of period T, the phase difference ϕ_n is given by

$$\phi_n = 2\pi \frac{\Delta t_n}{T} = \frac{4\pi n f L}{v} \quad . \tag{5.2}$$

Thus, the relative phase variation of the n^{th} echo is

$$\frac{\Delta \phi_n}{\phi_n} = \frac{\Delta f}{f} + \frac{\Delta L}{L} - \frac{\Delta v}{v} \quad . \tag{5.3}$$

During the measurement, the phase difference is kept to zero by adjusting the frequency of the rf signal. Thus, the relative change in the sound velocity is equal to

$$\frac{\Delta v}{v} = \frac{\Delta f}{f} + \frac{\Delta L}{L} \quad . \tag{5.4}$$

In general, as the relative change in the crystal's length $\frac{\Delta L}{L}$ is an order magnitude smaller than that of $\frac{\Delta v}{v}$, Eq. 5.5 constitutes a good approximation,

$$\frac{\Delta v}{v} \cong \frac{\Delta f}{f} \quad . \tag{5.5}$$

This last relation shows that the relative change in velocity, due to external parameters, can be directly measured from the relative change in frequency used to maintained the phase difference to zero.

5.3 Uniaxial Pressure Device

The main focus of this project is to study the effect of uniaxial pressure on the elastic properties of RLHS. For that purpose, we designed a sample holder where a uniaxial pressure is produced by means of a piezo-actuator (Physik Instrumente) which generate a blocking force of 800 N for an applied voltage of + 120 V. According to the study of Wu et al. [14] it has been reported that Landau model quantitatively describes both the temperature and pressure dependence of the elastic properties of RLHS in the tetragonal phase. However, due to the existence of the ferroelastic domains in the monoclinic phase of RLHS deviations from the model predictions are observed [14]. In the monoclinic phase of RLHS there are two ferroelastic domains perpendicular to each other. Since domains are present, the ultrasonic velocity data cannot be used to get the accurate values of the elastic constants in that phase. For an accurate determination of the elastic constants in monoclinic phase we have to do the ultrasonic measurements with a monodomain sample. In RLHS, domains lie in planes (100) and (010). Hence an application of normal stress along [100] or [010] should convert the sample into monodomain. Therefore, in this project we performed the ultrasonic measurements using sample under stress. We applied stress along [100] or [010] and measuremed the velocity along the [001] direction. We also realized velocity measurements along [001] without the stress for comparison. We also did velocity measurements along [010] with the stress along [100]. To produce the uniaxial stress the sample was mounted between two piezo-actuators. Measurements

without stress were done by leaving a clear gap between the actuators and the sample. The schematic diagram of the sample actuator assembly is shown in Fig. 5.4.

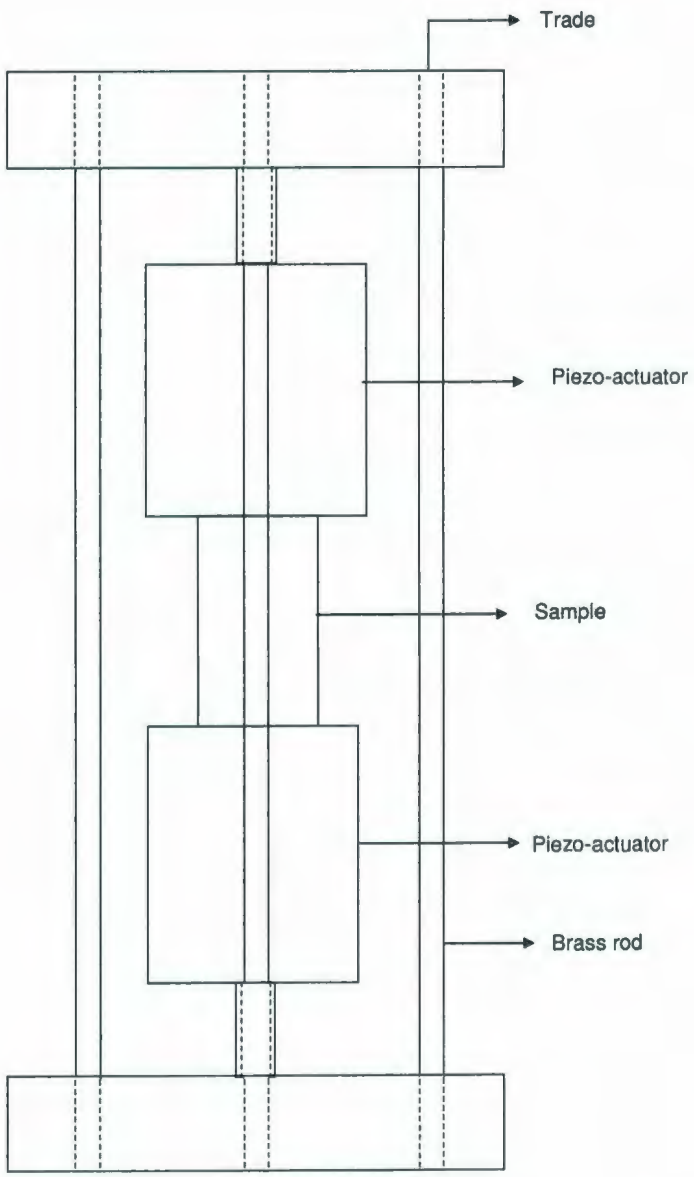

Figure 5.4: Schematic diagram of the sample actuator assembly in order to generate a uniaxial stress.

Chapter 6

Landau Model

Landau model can effectively be used to explain the major features associated with continuous phase transitions (second order). The thermodynamic state of any physical system is normally defined in terms of a Gibbs free energy which can be an explicit function of temperature T, pressure P, and volume V. A thermodynamic state is stable or metastable when the Gibbs free energy corresponds to a local minimum value. Thus, whenever pressure, temperature, stress or any other external physical parameter is changed, deviation in the Gibbs free energy can lead to a phase transformation [43]. The Gibbs free energy is defined as

$$G = U - TS + PV \ . \tag{6.1}$$

where U is the internal energy of the system, T is the absolute temperature, S is the entropy, P is the pressure, and V is the volume. Using the differential form of the internal energy given by

$$dU = TdS - PdV, \tag{6.2}$$

the total derivative of Gibbs free energy can be expressed as

$$dG = -SdT + VdP \ . \tag{6.3}$$

Thus, according to this result, the volume and entropy of the system can be obtained from the first partial derivatives of the Gibbs free energy,

$$V = \left(\frac{\partial G}{\partial P}\right)_T \quad ; \quad S = -\left(\frac{\partial G}{\partial T}\right)_P \quad . \tag{6.4}$$

Thus, during a phase transformations if a discontinuous variation in volume or entropy is found; the phase transition is labelled as first order or discontinuous [45]. Therefore, phase transitions from solid to liquid, gas to solid or liquid to gas are typical examples of first order phase transition, where a discontinuous volume change is observed at the critical point. In the case of second order or continuous phase transitions, the derivatives of the thermodynamic potentials are continuous, while the second derivative of the Gibbs free energy are discontinuous [45].

Taking the second derivative of the Gibbs free energy, we can define two physical parameters: the heat capacity at constant pressure c_p, and the compressibility at constant temperature α, where

$$c_P = T\left(\frac{\partial S}{\partial T}\right)_P = -T\left(\frac{\partial^2 G}{\partial T^2}\right)_P \tag{6.5}$$

$$\alpha = -\frac{1}{V}\left(\frac{\partial V}{\partial P}\right)_T = -\frac{1}{V}\left(\frac{\partial^2 G}{\partial P^2}\right)_T \quad . \tag{6.6}$$

In light of the heat capacity at constant pressure or the compressibility at constant temperature, a phase transition will be second order if there is discontinuity in any of the second derivatives of the free energy [43]. These different thermodynamic behaviours can be demonstrated experimentally by studying physical quantities in the vicinity of the transition.

6.1 Landau Theory

As the nature of the phase transition in RLHS is continuous, our discussion about the Landau model will be limited to continuous phase transitions. Landau theory

is a simple phenomenological thermodynamic model that is widely used to elucidate phase transitions. During a continuous phase transition a change in the symmetry of the material generally takes place, where the low symmetry phase is a subgroup of the high symmetry phase.

Basically, Landau theory is based on the concept that the free energy can be expanded as a function of a parameter called the order parameter. Now let us discuss briefly about the Landau order parameter first. This order parameter is a physical quantity which is used to distinguish the high symmetry phase from the low symmetry phase. Thus, this order parameter is zero in the high symmetry phase, while it must change continuously in the low symmetry phase. Thus, the excess Gibbs free energy, G is expressed as an infinite power series of the order parameter Q such that

$$G = \alpha_1 Q + \frac{1}{2}\alpha_2 Q^2 + \frac{1}{3}\alpha_3 Q^3 + \frac{1}{4}\alpha_4 Q^4 + \frac{1}{5}\alpha_5 Q^5 + \ldots \quad . \tag{6.7}$$

Considering that, for a second order phase transition, odd power terms in Q are not allowed [39, 43, 44] the expansion of the excess Gibbs free energy reduces to

$$G = \frac{1}{2}\alpha_2 Q^2 + \frac{1}{4}\alpha_4 Q^4 \tag{6.8}$$

where higher power terms are neglected. A state will be stable only when the excess Gibbs free energy corresponds to a local minimum, i.e., the first derivative with respect to the order parameter Q must be zero, while the second derivative must be larger than zero

$$\frac{\partial G}{\partial Q} = \alpha_2 Q + \alpha_4 Q^3 = 0 \ , \tag{6.9}$$

$$\frac{\partial^2 G}{\partial Q^2} = \alpha_2 + 3\alpha_4 Q^2 > 0 \ . \tag{6.10}$$

Since the value of order parameter Q is zero in the high symmetry phase, Eq. 6.10 indicates that α_2 must be positive in the high temperature phase. However, in the

low symmetry phase we find (see Eq. 5.10) that α_2 is negative as we must impose that $\alpha_4 > 0$. Thus, at the transition temperature T_c we note that α_2 changes sign. For that reason, Landau postulates that the temperature dependence of α_2 is simply

$$\alpha_2 = a(T - T_c) \tag{6.11}$$

where the coefficient a is a positive constant. Hence, the excess Gibbs free energy can be expressed as

$$G = \frac{1}{2}a(T - T_c)Q^2 + \frac{1}{4}\alpha_4 Q^4 \quad . \tag{6.12}$$

Taking the first derivative of Eq. 6.12 with respect to Q and setting it equal to zero, we find that

$$Q = 0, \qquad T > T_c \tag{6.13}$$

$$Q = \sqrt{\frac{a}{\alpha_4}(T_c - T)}, \qquad T < T_c \quad . \tag{6.14}$$

Fig. 5.1 shows the temperature dependence of the order parameter. We see that the order parameter vanishes above the transition temperature. The order parameter appears at $T = T_c$ and increases continuously as $(T - T_c)^{\frac{1}{2}}$ below T_c.

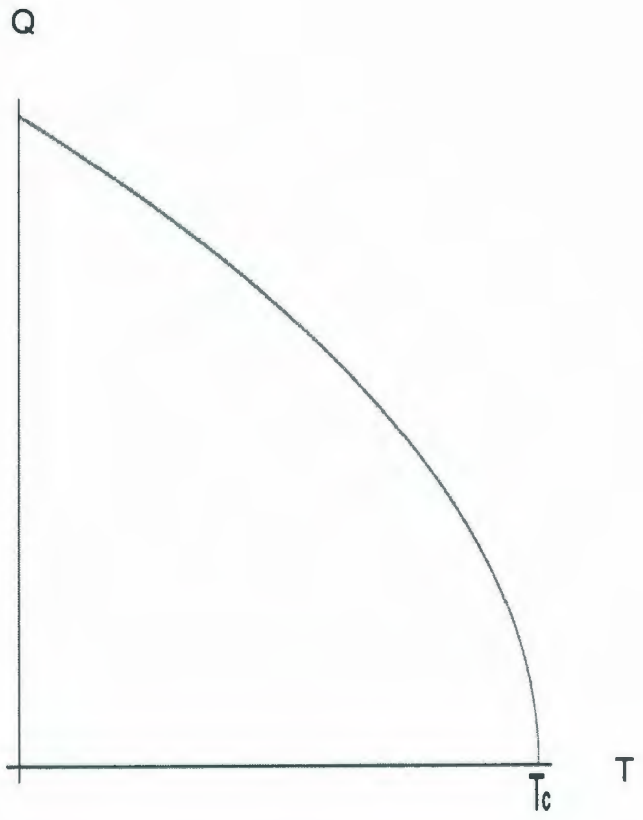

Figure 6.1: Schematic plot of order parameter, Q as a function of temperature. Q vanishes in the high symmetry phase and increases continuously as $(T - T_c)^{\frac{1}{2}}$ in the low symmetry phase.

Chapter 7

Landau Analysis

In a Landau model, the excess Gibbs free energy is used to differentiate the low symmetry phase from the high symmetry phase in terms of an order parameter. In the high symmetry phase the order parameter is zero while it is non-zero in the low symmetry phase. This free energy can also be expanded, by adding coupling terms between the order parameter and strains in order to obtain analytical solutions of the elastic properties. Thus, in this chapter we present different Landau models which should account for the pressure dependence of the elastic properties of $Rb_4LiH_3(SO_4)_4$. In particular, we consider three distinct cases: hydrostatic pressure, uniaxial pressure applied along the z-axis, and a uniform pressure applied in the xy-plane.

In the absence of an external pressure, the Landau free energy expansion is given by

$$F = F_L + F_{el} + F_c \quad . \tag{7.1}$$

The first term F_L is the Landau expansion of the Gibbs free energy that depends on the Landau order parameter Q,

$$F_L = \frac{1}{2}AQ^2 + \frac{1}{4}BQ^4 \tag{7.2}$$

where A is a temperature dependent Landau coefficient [46] defined as

$$A = \alpha(T - T_0) \quad . \tag{7.3}$$

The second contribution F_{el} is the elastic energy associated with the elastic deformations defined in terms of the strain components e_α,

$$\begin{aligned} F_{el} = \frac{1}{2}C_{11}({e_1}^2 + {e_2}^2) + \frac{1}{2}C_{44}({e_4}^2 + {e_5}^2) + \frac{1}{2}C_{33}{e_3}^2 \\ + \frac{1}{2}C_{66}{e_6}^2 + C_{12}e_1e_2 + C_{13}(e_1 + e_2)e_3 + C_{16}(e_1 - e_2)e_6 \end{aligned} \tag{7.4}$$

where the elastic constants are those of the paraelastic phase (tetragonal 4 point group, Eq. 4.35). Finally, the third term F_c considers the coupling energy between the strain components e_α and the order parameter Q. The allowed coupling terms can be easily identified based of symmetry considerations. The lowest order coupling terms considered here are

$$F_c = \beta Q(e_1 - e_2) + \gamma Q e_6 + \delta Q^2 e_3 + \lambda Q^2(e_1 + e_2) + \zeta e_4 e_5 Q + \eta({e_4}^2 - {e_5}^2)Q \tag{7.5}$$

where β, γ, δ, λ, ζ and η are the coupling coefficients to be calculated later [14].

In the high symmetry phase RLHS belongs to the point group symmetry 4 [42]. Thus, all terms in the free energy must remain invariant under the symmetry operation ${C_4}^1$, corresponding to a rotation of 90° of the crystal. Since the order parameter has the same symmetry as the spontaneous strains $(e_1 - e_2)$ and e_6, bilinear coupling terms $\beta Q(e_1 - e_2)$ and $\gamma Q e_6$ are allowed. Table 7.1 represents how the strain components transform under the symmetry operation ${C_4}^1$. Using the transformations listed in Table 7.1 it is easy to verify that all terms considered in Eq. 7.4-7.5 are indeed invariant.

Table 7.1: Transformations of the strain components under the symmetry operation $C_4{}^1$ in the high symmetry phase of RLHS.

Strain components	e_1	e_2	e_3	e_4	e_5	e_6
Symmetry operation, $C_4{}^1$	e_2	e_1	e_3	$-e_5$	e_4	$-e_6$

7.1 Calculations for a Hydrostatic Pressure

In the present case, we consider a hydrostatic pressure where the energy due to pressure is given by

$$F_{P(Hydro)} = P(e_1 + e_2 + e_3) \ . \tag{7.6}$$

Let point out that this pressure energy is also invariant under the symmetry operation. Combining all contributions, the total free energy expansion is

$$\begin{aligned} F_1 = &\frac{1}{2}AQ^2 + \frac{1}{4}BQ^4 + \frac{1}{2}C_{11}({e_1}^2 + {e_2}^2) + \frac{1}{2}C_{44}({e_4}^2 + {e_5}^2) \\ &+\frac{1}{2}C_{33}{e_3}^2 + C_{12}e_1e_2 + C_{13}(e_1 + e_2)e_3 + C_{16}(e_1 - e_2)e_6 \\ &+\beta Q(e_1 - e_2) + \gamma Qe_6 + \delta Q^2e_3 + \lambda Q^2(e_1 + e_2) + \zeta e_4e_5Q \\ &+\eta({e_4}^2 - {e_5}^2)Q + P(e_1 + e_2 + e_3) \ . \end{aligned} \tag{7.7}$$

This expression can be used to calculate the strains, the order parameter, the pressure dependence of the transition temperature, and the elastic constants.

The equilibrium condition for the free energy is given by

$$\frac{\partial F_1}{\partial e_\alpha} = 0 \tag{7.8}$$

where α extends from 1 to 6. Using Eq. 7.8, we obtain six equations which can be solved to obtain the strain components e_α as a function of P and Q. The strain components correspond to

$$e_1 - e_2 = \frac{2\left(\gamma C_{16} - \beta C_{66}\right)}{C_d}Q \tag{7.9}$$

$$e_1 + e_2 = \frac{2\left(\delta C_{13} - \lambda C_{33}\right)}{C_a} Q^2 - \frac{2\left(C_{33} - C_{13}\right)}{C_a} P \tag{7.10}$$

$$e_3 = \frac{\delta\left(C_{11} + C_{12}\right) - 2\lambda C_{13}}{C_a} Q^2 - \frac{C_g}{C_a} P \tag{7.11}$$

$$e_4 = 0 \tag{7.12}$$

$$e_5 = 0 \tag{7.13}$$

$$e_6 = -\frac{\gamma\left(C_{11} - C_{12}\right) - 2\beta C_{16}}{C_d} Q \tag{7.14}$$

where C_a, C_d and C_g are defined by

$$C_a = \left(C_{11} + C_{12}\right) C_{33} - 2{C_{13}}^2 \,, \tag{7.15}$$

$$C_d = \left(C_{11} - C_{12}\right) C_{66} - 2{C_{16}}^2 \,, \tag{7.16}$$

$$C_g = C_{11} + C_{12} - 2C_{13} \,. \tag{7.17}$$

According to Eq. 7.9 and Eq. 7.14, it is clear that $(e_1 - e_2)$ and e_6 have the same symmetry properties as the order parameter, Q.

Minimizing the free energy Eq. 7.7 with respect to the order parameter Q, we get

$$\begin{aligned} \frac{\partial F_1}{\partial Q} &= Q\left(T - T_0\right)\alpha + Q^3 A_4 + \beta\left(e_1 - e_2\right) \\ &+2Q\lambda\left(e_1 + e_2\right) + 2Q\delta e_3 + \zeta e_4 e_5 + \eta\left({e_4}^2 - {e_5}^2\right) + \gamma e_6 = 0 \end{aligned} \tag{7.18}$$

Making use of the expressions for e_α in Eq. 7.18 and solving for the order parameter Q, we obtain the solution for Q as a function of P and T. The expression for the order parameter is given by Eq. 7.19, which is similar to the mean field dependence derived in Chapter 6, Eq. 6.14.

$$Q(T,P) = \sqrt{\frac{\alpha C_a\left(T_c + \frac{dT_c}{dP} P - T\right)}{\Delta}} \,, \tag{7.19}$$

$$T_c = T_0 + \frac{C_b}{\alpha C_d} \,, \tag{7.20}$$

$$\frac{dT_c}{dP} = 2\frac{C_c}{\alpha C_a} \ , \tag{7.21}$$

where

$$C_b = \gamma^2 \left(C_{11} - C_{12}\right) + 2\beta \left(\beta C_{66} - 2\gamma C_{16}\right) \ , \tag{7.22}$$

$$C_c = \delta \left(C_{11} + C_{12} - 2C_{13}\right) + 2\lambda \left(C_{33} - 2C_{13}\right) \ , \tag{7.23}$$

$$\Delta = A_4 C_a - 4\lambda^2 C_{33} - 2\left(C_{11} + C_{12}\right)\delta^2 + 8\delta\lambda C_{13} \ . \tag{7.24}$$

At zero pressure the expression for the critical temperature is given as

$$T_c\left(P = 0\right) = T_0 + \frac{-\gamma^2 C_{11} + \gamma^2 C_{12} + 4\beta\gamma C_{16} - 2\beta^2 C_{66}}{\alpha\left(2{C_{16}}^2 + \left(C_{12} - C_{11}\right) C_{66}\right)} \ . \tag{7.25}$$

In the case of hydrostatic pressure, the expression for the pressure dependence of the transition temperature is given by

$$\frac{dT_c}{dP} = -\frac{2\left(\delta C_{11} + \delta C_{12} - 2\delta C_{13} - 2\lambda C_{13} + 2\lambda C_{33}\right.}{\alpha\left(2{C_{13}}^2 - \left(C_{11} + C_{12}\right) C_{33}\right)} \ . \tag{7.26}$$

7.2 Calculations for a Uniform Pressure Acting in the xy-plane

In this section we assume a uniform pressure acting in the xy-plane. In that case, the energy due to a pressure is given by

$$F_{P(XY)} = P(e_1 + e_2) \ . \tag{7.27}$$

This pressure energy is also invariant under the symmetry operation in the high temperature phase. Combining all contributions, the overall expression for the free

energy is given by

$$\begin{aligned} F_2 = &\frac{1}{2}AQ^2 + \frac{1}{4}BQ^4 + \frac{1}{2}C_{11}({e_1}^2 + {e_2}^2) + \frac{1}{2}C_{44}({e_4}^2 + {e_5}^2) \\ &+\frac{1}{2}C_{33}{e_3}^2 + C_{12}e_1e_2 + C_{13}(e_1 + e_2)e_3 + C_{16}(e_1 - e_2)e_6 \\ &+\beta Q(e_1 - e_2) + \gamma Q e_6 + \delta Q^2 e_3 + \lambda Q^2(e_1 + e_2) + \zeta e_4 e_5 Q \\ &+\eta({e_4}^2 - {e_5}^2)Q + P(e_1 + e_2)\ . \end{aligned} \tag{7.28}$$

Using the minimization condition (given in Eq. 7.8) with the free energy F_2 (Eq. 7.28), we obtain

$$e_1 - e_2 = \frac{2\left(\gamma C_{16} - \beta C_{66}\right)}{\left(C_{11} - C_{12}\right)C_{66} - 2{C_{16}}^2} Q \tag{7.29}$$

$$e_1 + e_2 = -\frac{2\left(-Q^2\delta C_{13} + \left(P + Q^2\lambda\right)C_{33}\right)}{\left(C_{11} + C_{12}\right)C_{33} - 2{C_{13}}^2} \tag{7.30}$$

$$e_3 = \frac{2PC_{13}}{\left(C_{11} + C_{12}\right)C_{33} - 2{C_{13}}^2} - \frac{Q^2\left(\delta C_{11} + \delta C_{12} - 2\lambda C_{13}\right)}{\left(C_{11} + C_{12}\right)C_{33} - 2{C_{13}}^2} \tag{7.31}$$

$$e_4 = 0 \tag{7.32}$$

$$e_5 = 0 \tag{7.33}$$

$$e_6 = -\frac{\gamma\left(C_{11} - C_{12}\right) - 2\beta C_{16}}{\left(C_{11} - C_{12}\right)C_{66} - 2{C_{16}}^2} Q\ . \tag{7.34}$$

Investigating Eq. 7.29 and Eq. 7.34, we observe that $(e_1 - e_2)$ and e_6 have the same symmetry as that of the order parameter Q.

Again using the minimization of the free energy F_2 with respect to Q, we obtain

$$\begin{aligned} \frac{\partial F_2}{\partial Q} = &Q\left(T - T_0\right)\alpha + Q^3 A_4 + \beta\left(e_1 - e_2\right) + 2Q\lambda\left(e_1 + e_2\right) \\ &+2Q\delta e_3 + \zeta e_4 e_5 + \eta\left({e_4}^2 - {e_5}^2\right) + \gamma e_6 = 0\ . \end{aligned} \tag{7.35}$$

Plugging in the expressions of e_α in Eq. 7.35, we obtain the solution for the order parameter Q as a function of T and P. In this case the expression of the order parameter is given by

$$Q(T,P) = \sqrt{\frac{\alpha C_a\left(T_c + \frac{dT_c}{dP}P - T\right)}{\Delta}}\ , \tag{7.36}$$

with same Δ and C_a as before. where

$$\frac{dT_c}{dP} = 4\frac{C_e}{\alpha C_a} , \tag{7.37}$$

$$C_e = \delta C_{13} - \lambda C_{33} \ . \tag{7.38}$$

The pressure dependence of the transition temperature for a uniform pressure acting in the xy-plane of the crystal is given by

$$\frac{dT_c}{dP} = \frac{4\delta C_{13} - 4\lambda C_{33}}{\alpha\left(2{C_{13}}^2 - (C_{11} + C_{12})\, C_{33}\right)} \ . \tag{7.39}$$

7.3 Calculations for a Uniaxial Pressure Applied Along the z-direction

The energy due to a uniaxial pressure applied along the z-direction is written as

$$F_{P(Z)} = Pe_3, \tag{7.40}$$

which is invariant under the symmetry operation. Therefore, the overall free energy is

$$\begin{aligned} F_3 = {} & \frac{1}{2}AQ^2 + \frac{1}{4}BQ^4 + \frac{1}{2}C_{11}({e_1}^2 + {e_2}^2) + \frac{1}{2}C_{44}({e_4}^2 + {e_5}^2) \\ & + \frac{1}{2}C_{33}{e_3}^2 + C_{12}e_1e_2 + C_{13}(e_1 + e_2)e_3 + C_{16}(e_1 - e_2)e_6 \\ & + \beta Q(e_1 - e_2) + \gamma Q e_6 + \delta Q^2 e_3 + \lambda Q^2(e_1 + e_2) + \zeta e_4 e_5 Q \\ & + \eta({e_4}^2 - {e_5}^2)Q + Pe_3 \ . \end{aligned} \tag{7.41}$$

As previously the solutions for the spontaneous strains are found by minimizing the free energy F_3 with respect to e_α

$$\frac{\partial F_3}{\partial e_\alpha} = 0 \ . \tag{7.42}$$

Solving Eq. 7.42, we obtain the six components of the spontaneous strains which correspond to

$$e_1 - e_2 = \frac{2\left(\gamma C_{16} - \beta C_{66}\right)}{\left(C_{11} - C_{12}\right) C_{66} - 2{C_{16}}^2} Q \tag{7.43}$$

$$e_1 + e_2 = -\frac{2\left(\left(P + Q^2\delta\right) C_{13} - Q^2 \lambda C_{33}\right)}{\left(C_{11} + C_{12}\right) C_{33} - 2{C_{13}}^2} \tag{7.44}$$

$$e_3 = \frac{P\left(C_{11} + C_{12}\right)}{\left(C_{11} + C_{12}\right) C_{33} - 2{C_{13}}^2} - \frac{Q^2\left(\delta C_{11} + \delta C_{12} - 2\lambda C_{13}\right)}{\left(C_{11} + C_{12}\right) C_{33} - 2{C_{13}}^2} \tag{7.45}$$

$$e_4 = 0 \tag{7.46}$$

$$e_5 = 0 \tag{7.47}$$

$$e_6 = -\frac{\gamma\left(C_{11} - C_{12}\right) - 2\beta C_{16}}{\left(C_{11} - C_{12}\right) C_{66} - 2{C_{16}}^2} Q \ . \tag{7.48}$$

The solution for the order parameter can be calculated from the minimization of the free energy with respect to Q,

$$\begin{aligned} \frac{\partial F_3}{\partial Q} = {} & Q\left(T - T_0\right)\alpha + Q^3 A_4 + \beta\left(e_1 - e_2\right) + 2Q\lambda\left(e_1 + e_2\right) \\ & + 2Q\delta e_3 + \zeta e_4 e_5 + \eta\left({e_4}^2 - {e_5}^2\right) + \gamma e_6 = 0 \ . \end{aligned} \tag{7.49}$$

Using the expressions for e_α in Eq. 7.49, we find the expression of the order parameter. In this case, the expression of Q can be also written as the above two expressions of the Q given in Eq. 7.19 and Eq. 7.36, with a difference only in their pressure dependence of T_c.

$$Q(T, P) = \sqrt{\frac{\alpha C_a\left(T_c + \frac{dT_c}{dP} P - T\right)}{\Delta}} \ , \tag{7.50}$$

where

$$\frac{dT_c}{dP} = 2\frac{C_f}{\alpha C_a} \ , \tag{7.51}$$

$$C_f = 2(\delta(C_{13} + C_{12}) - 2\lambda C_{13}) \ . \tag{7.52}$$

In the case of a uniaxial pressure acting along the z-direction the transition temperature varies according to the following relation

$$\frac{dT_c}{dP} = -\frac{2(\delta C_{11} + \delta C_{12} - 2\lambda C_{11})}{\alpha\left(2{C_{13}}^2 - \left(C_{11} + C_{12}\right) C_{33}\right)} \ . \tag{7.53}$$

7.4 Calculations of the Coupling Parameters

Elastic properties of RLHS have been measured by ultrasonic velocity measurements [10] and Brillouin scattering experiments [7] and the results have already been analyzed. Thus, in this project we use the published elastic constants. Table 7.2 shows the values of the bare elastic constants for RLHS in the paraelastic phase. Using

Table 7.2: The values of the bare elastic constants for RLHS in the paraelastic phase.

Elastic Constants	$\times 10^{10}$ N/m^2
$C_{11}{}^0$	4.95
$C_{12}{}^0$	1.77
$C_{13}{}^0$	2.00
$C_{16}{}^0$	-0.15
$C_{33}{}^0$	5.14
$C_{44}{}^0$	0.74
$C_{55}{}^0$	1.10

Raman scattering measurements in RLHS, Oktay et al. [48] were also able to estimate the coupling strength between the soft acoustic and optical mode, which has been found to be $T_c - T_0 = 900$ K. Thus, to calculate the coupling coefficients, we also use the pressure dependence of the transition temperature and the temperature dependence of the spontaneous strains [12] which must satisfy

$$T_c - T_0 = \frac{C_b}{\alpha C_d} = 900 \text{ K} , \tag{7.54}$$

$$\frac{dT_c}{dP} = 2\frac{C_c}{\alpha C_a} = 191 \text{ K/GPa}, \tag{7.55}$$

$$\frac{e_1 - e_2}{e_6} = -\frac{2\left(\gamma C_{16} - \beta C_{66}\right)}{\gamma\left(C_{11} - C_{12}\right) - 2\beta C_{16}} = 3 , \tag{7.56}$$

$$e_6\,(0K) = -\frac{\gamma\,(C_{11} - C_{12}) - 2\beta C_{16}}{C_d} Q_0 = 0.0096\ , \tag{7.57}$$

$$e_3\,(0K) = -\frac{\delta\,(C_{11} + C_{12}) - 2\lambda C_{13}}{C_a} {Q_0}^2 = -0.0016\ , \tag{7.58}$$

$${Q_0}^2 \approx \frac{\alpha T_c}{A_4}\ . \tag{7.59}$$

Setting the standard value of $\alpha = 1.07 \times 10^9$ and solving this set of relations, we obtain the following values of the coupling parameters listed in Table 7.3. In order to reproduce the experimental values of the elastic constants C_{44} and C_{45}, we set the values of the last two coupling parameters η and ζ accordingly.

Table 7.3: Coupling parameters of RLHS in the high symmetry (tetragonal) phase.

Coupling parameters	Values
α	1.07×10^{9}
A_4	4.86×10^{15}
β	8.17×10^{10}
γ	-1.15×10^{10}
λ	2.70×10^{12}
δ	3.75×10^{12}
η	-1.00×10^{10}
ζ	2.00×10^{10}

7.5 Pressure Dependence of the Transition Temperature

Plugging in the values of coupling parameters given in Table 7.3, the values of bare elastic constants of RLHS listed in Table 7.2, and the value of T_0, we obtain the

pressure dependence of the transition temperature for each cases,

$$T_c\left(P_{(Hydro)}\right) = 134 + 1.91 \times 10^{-7} P \ , \tag{7.60}$$

$$T_c\left(P_{(XY)}\right) = 134 + 0.90 \times 10^{-7} P \ , \tag{7.61}$$

$$T_c\left(P_{(Z)}\right) = 134 + 1.01 \times 10^{-7} P \ . \tag{7.62}$$

We observe that the transition temperature of RLHS increases linearly with the application of stress. Furthermore, we also notice that, for the same amount of applied pressure the increase in transition temperature is the largest for the hydrostatic pressure and the lowest for a pressure applied along the xy-plane.

7.6 Temperature Depedence of the Order Parameter at Various Stresses

In 1950, the term order parameter was introduced by Ginzburg and Landau in their phenomenological theory to discuss the ordering phenomena around a phase transition [47]. In the high symmetry phase the order parameter is zero and in the low symmetry phase the order parameter has a non-zero value. Here we present the temperature dependence of the order parameter of RLHS for a hydrostatic pressure, a uniform pressure acting in the xy plane and a uniaxial pressure along the z-direction. Fig. 7.1 shows the temperature dependence of order parameter at zero and 8 kbar (800 MPa). In the low symmetry phase, the magnitude of the order parameter increases significantly with the application of pressure, principally due to an increase in the critical temperature. The order parameter at $T = 0$ K has its maximum value for the hydrostatic pressure and minimum value for a pressure applied into the xy plane.

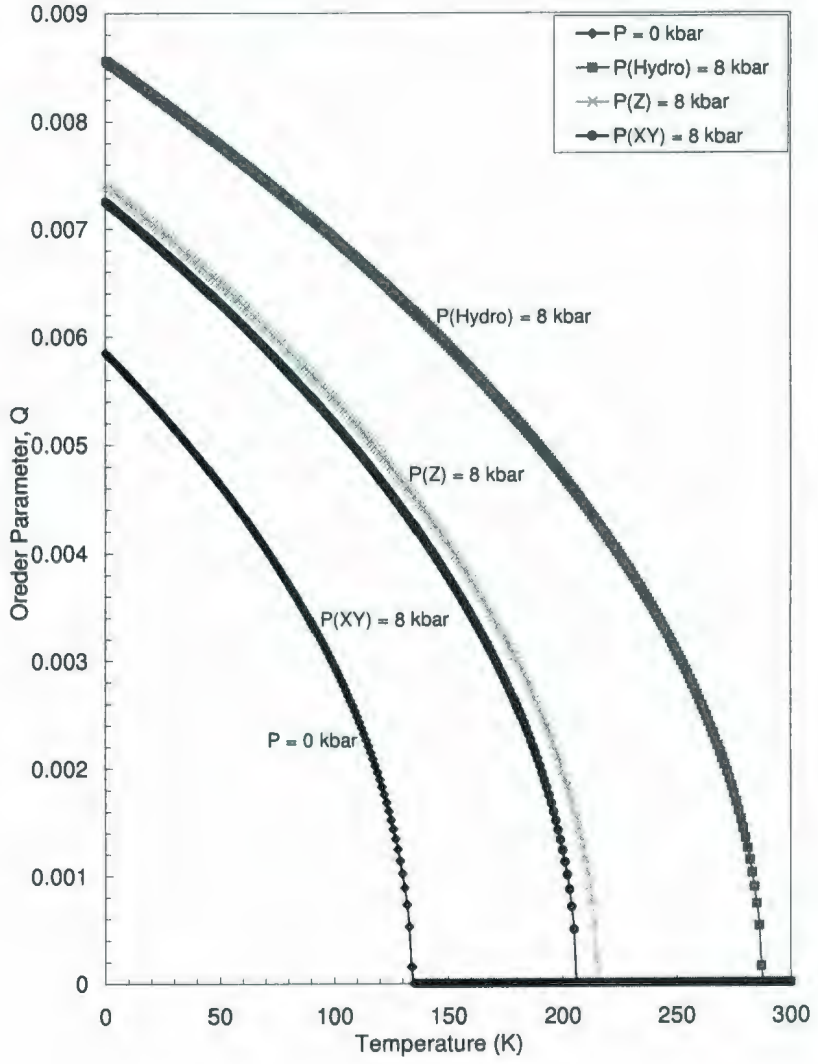

Figure 7.1: Temperature dependence of the order parameter at various pressures.

7.7 Temperature Dependence of the Strain Components at Various Pressures

Fig. 7.2 and Fig. 7.3 show the effect of a hydrostatic pressure, xy pressure, and a uniaxial pressure on the strain components e_1, e_2, and e_3 below and above the transition temperature. At zero pressure the strain components e_2, and e_3 decrease monotonically with cooling below T_c, while e_1 increases.

Whenever a hydrostatic pressure of 8 kbar (800 MPa) is applied along the three perpendicular axes of the sample, the magnitude of strain components e_1, e_2 and e_3 decreases with pressure. This is because with the application of a hydrostatic pressure the sample gets deformed and is contracted along x, y and z-directions. Meanwhile, if the pressure is applied into the xy-plane, the x and y-directions contract while the the z-direction expands ($e_3 > 0$). Similar behaviour is observed whenever a uniaxial pressure of 8 kbar (800 MPa) is applied along the z-direction. In that case the sample expands along the x and y-directions while it contracts along the z-direction ($e_3 < 0$).

Let us now examine the pressure dependence of the spontaneous strain e_6 presented in Fig. 7.4. Since the order parameter is zero in the high symmetry phase, and considering that e_6 is proportional to the order parameter, e_6 is always zero above the transition temperature, regardless of the pressure. Thus, the strain component e_6 increases continuously as the temperature decreases below T_c. Moreover, we find that e_6 is larger for a hydrostatic pressure and lower for the xy pressure.

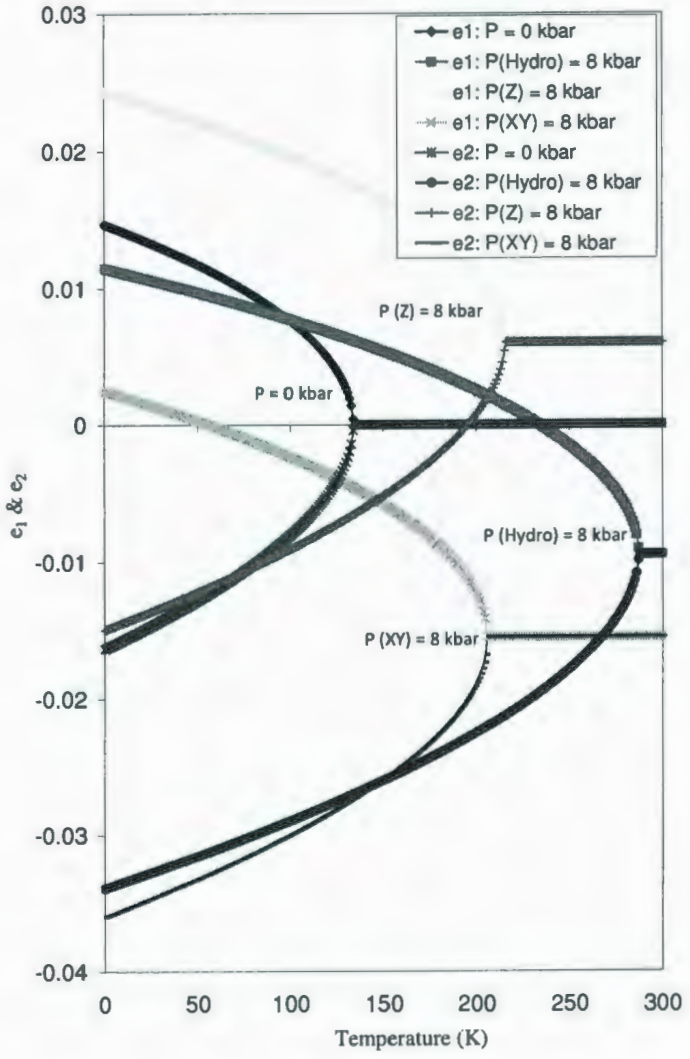

Figure 7.2: Temperature dependence of strain components e_1 and e_2 at various applied stresses.

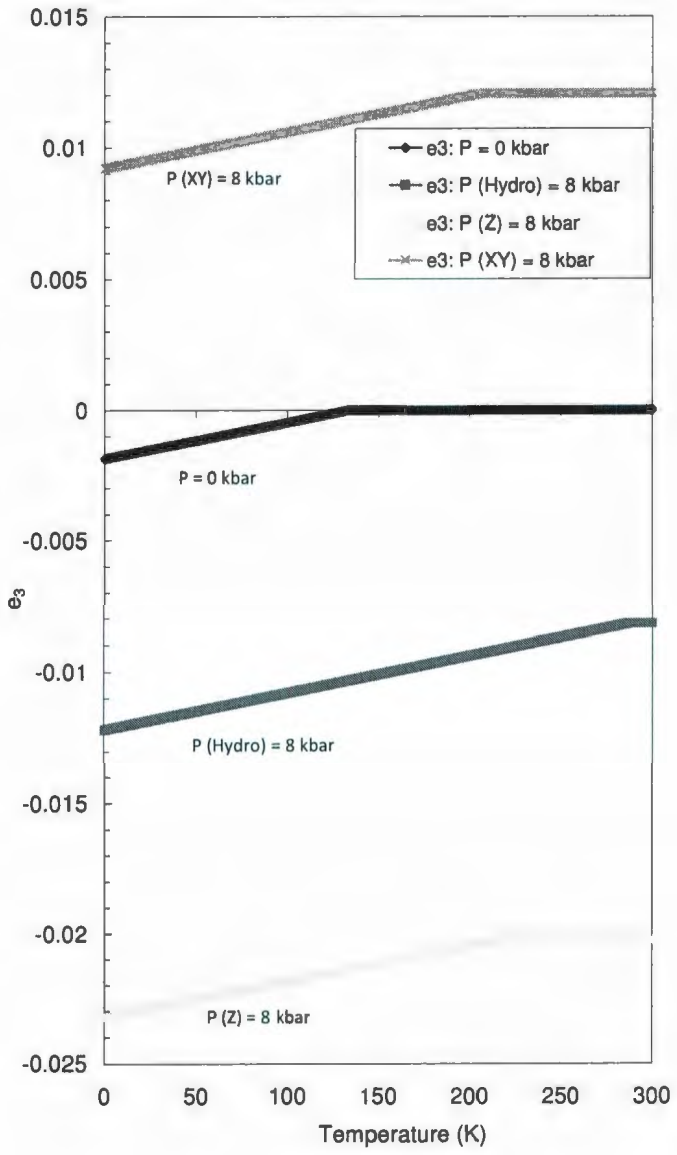

Figure 7.3: Temperature dependence of strain component e_3 at various applied stresses.

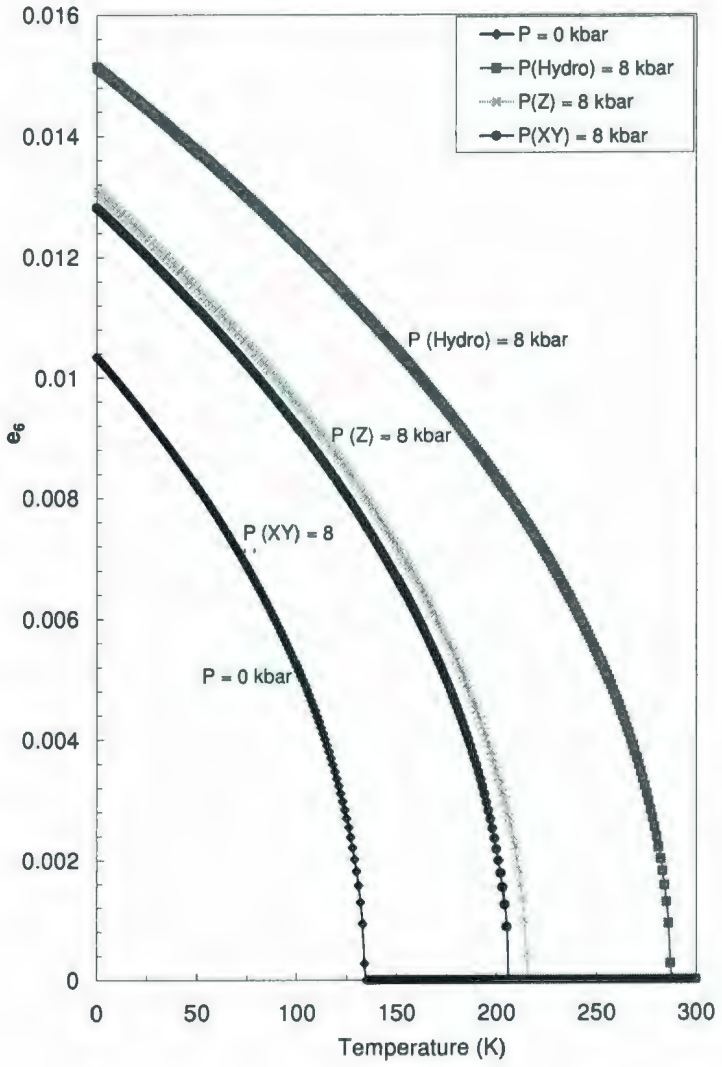

Figure 7.4: Temperature dependence of strain component e_6 at various applied stresses.

7.8 Pressure Dependence of Strain Components above T_c

It is well known that at zero pressure all strain components are zero above the transition temperature. As all numerical values of the bare elastic constants and coupling parameters are known, we can compare the effect of hydrostatic, xy, and uniaxial pressure on the strain components above the transition temperature. Fig. 7.5 and Fig. 7.6 show the pressure dependence of e_1, e_2, and e_3 at 300 K. From Fig. 7.5 and Fig. 7.6 we observe that the critical pressure of RLHS is 8 kbar (800 MPa) for a hydrostatic pressure. Moreover, below the critical pressure, e_1, e_2, and e_3 decrease continuously with pressure. At the critical pressure e_1 shows a sharp positive jump while e_2 exhibits a sharp negative jump.

Whenever we apply a xy pressure the strain components e_1 and e_2 display a behaviour similar to that described for a hydrostatic pressure, at a higher critical pressure of 18.4 kbar (1.84 GPa). However, in this case the strain component e_3 increases with pressure, indicating that the sample expands along the z-direction.

Finally, for a uniaxial pressure along the z-direction we observe that e_1 and e_2 increase linearly below the critical pressure. In this case the value of critical pressure for RLHS is 16 kbar (1.6 GPa). Around the critical pressure e_1 exhibits a clean positive jump while e_2 shows a small negative jump. On the other hand, the magnitude of e_3 decreases linearly.

As mentioned previously, the strain component e_6 possesses the same symmetry as the order parameter and thus, as shown in Fig. 7.7, it behaves like the order parameter as a function of pressure. For that reason, below the critical pressure the value of e_6 is zero.

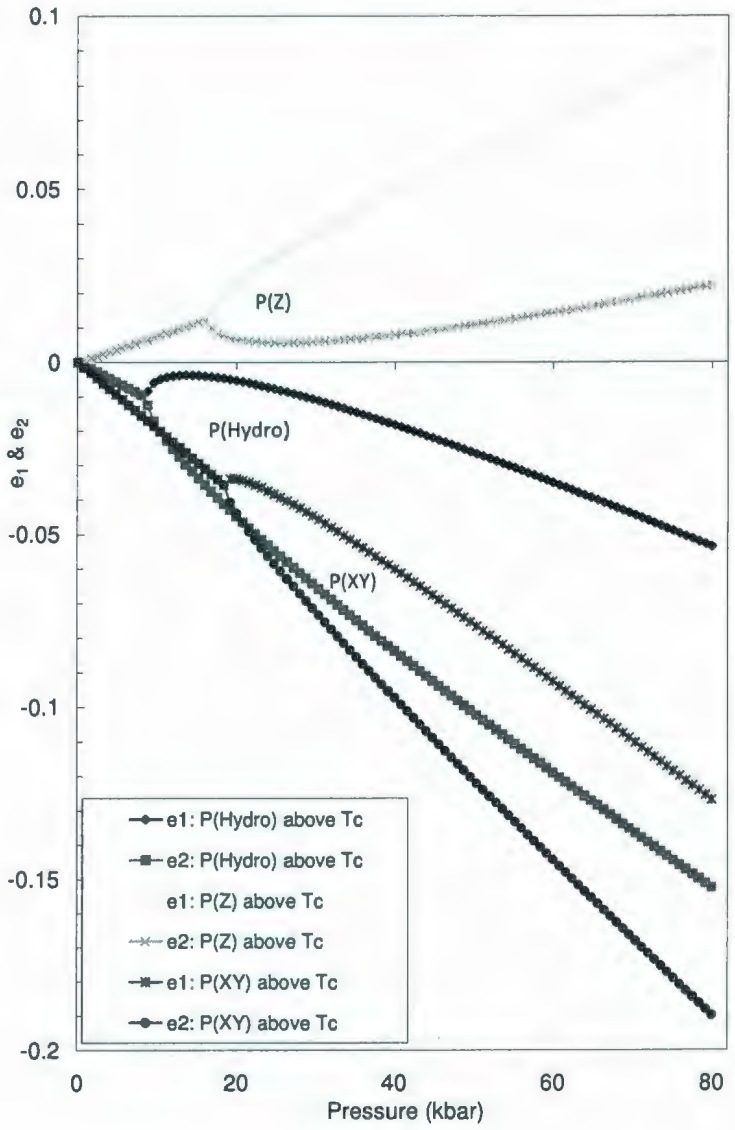

Figure 7.5: Pressure dependence of strain components e_1 and e_2 above T_c.

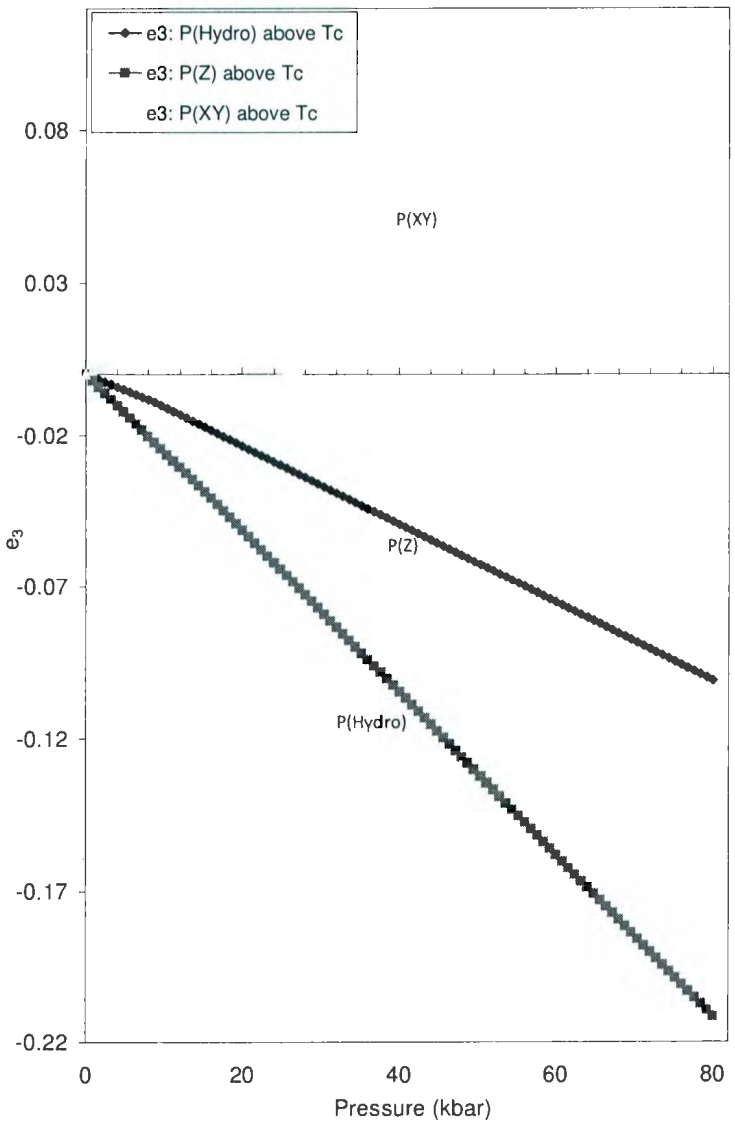

Figure 7.6: Pressure dependence of strain component e_3 above T_c.

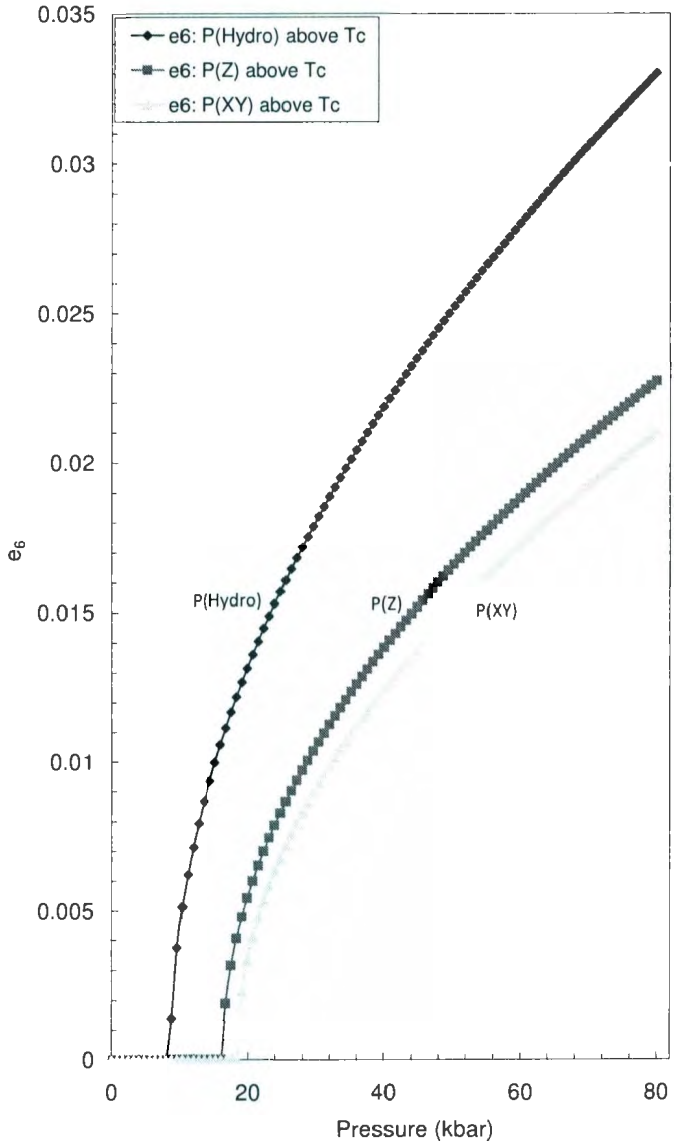

Figure 7.7: Pressure dependence of strain component e_6 above T_c.

7.9 Calculations of the Elastic Constants of RLHS Using Landau Model

In this section we describe the calculations of the elastic constants of RLHS in the light of the Landau model. Using the Landau model free energy (F_1, F_2, and F_3) the elastic constants of RLHS can be obtained using the relation [42]

$$C_{ij} = \left(\frac{\partial^2 F}{\partial e_i \partial e_j}\right) - \frac{\partial^2 F}{\partial Q \partial e_i}\left(\frac{\partial^2 F}{\partial Q^2}\right)^{-1}\left(\frac{\partial^2 F}{\partial e_j \partial e_Q}\right) \quad . \tag{7.63}$$

The expressions of the 13 independent elastic constants for all pressure scenarios can conveniently be written as

$$C_{11} = {C_{11}}^0 - \frac{(\beta + 2\lambda Q)^2}{\alpha(T_0 + T) + 3A_4Q^2 + 2\lambda(e_1 + e_2) + 2\delta e_3} \tag{7.64}$$

$$C_{22} = {C_{11}}^0 - \frac{(-\beta + 2\lambda Q)^2}{\alpha(T_0 + T) + 3A_4Q^2 + 2\lambda(e_1 + e_2) + 2\delta e_3} \tag{7.65}$$

$$C_{33} = {C_{33}}^0 - \frac{4Q^2\delta^2}{\alpha(T_0 + T) + 3A_4Q^2 + 2\lambda(e_1 + e_2) + 2\delta e_3} \tag{7.66}$$

$$C_{44} = {C_{44}}^0 + 2\eta Q \tag{7.67}$$

$$C_{55} = {C_{44}}^0 - 2\eta Q \tag{7.68}$$

$$C_{66} = {C_{66}}^0 - \frac{\gamma^2}{\alpha(T_0 + T) + 3A_4Q^2 + 2\lambda(e_1 + e_2) + 2\delta e_3} \tag{7.69}$$

$$C_{12} = {C_{12}}^0 - \frac{(\beta + 2\lambda Q)(2\lambda Q - \beta)}{\alpha(T_0 + T) + 3A_4Q^2 + 2\lambda(e_1 + e_2) + 2\delta e_3} \tag{7.70}$$

$$C_{13} = {C_{13}}^0 - \frac{2\delta Q(\beta + 2\lambda Q)}{\alpha(T_0 + T) + 3A_4Q^2 + 2\lambda(e_1 + e_2) + 2\delta e_3} \tag{7.71}$$

$$C_{16} = {C_{16}}^0 - \frac{\gamma(\beta + 2\lambda Q)}{\alpha(T_0 + T) + 3A_4Q^2 + 2\lambda(e_1 + e_2) + 2\delta e_3} \tag{7.72}$$

$$C_{23} = {C_{13}}^0 - \frac{2\delta Q(2\lambda Q - \beta)}{\alpha(T_0 + T) + 3A_4Q^2 + 2\lambda(e_1 + e_2) + 2\delta e_3} \tag{7.73}$$

$$C_{26} = -{C_{16}}^0 - \frac{\gamma(2\lambda Q - \beta)}{\alpha(T_0 + T) + 3A_4Q^2 + 2\lambda(e_1 + e_2) + 2\delta e_3} \tag{7.74}$$

$$C_{36} = -\frac{2\gamma\delta Q}{\alpha\left(T_0 + T\right) + 3A_4Q^2 + 2\lambda\left(e_1 + e_2\right) + 2\delta e_3} \tag{7.75}$$

$$C_{45} = \zeta Q \tag{7.76}$$

where $C_{\alpha\beta}{}^0$ are the elastic constants listed in Table 7.2. To obtain the corresponding expression in the tetragonal phase, we simply set the order parameter Q to zero. The specific temperature and pressure dependence are obtained by using the solutions of Q and e_α associated with a hydrostastic, xy, and uniaxial pressure.

7.10 Discussions on the Elastic Constants

In this section, we present the temperature dependence of the elastic constants of RLHS at zero and 8 kbar (800 MPa) for a hydrostatic pressure, a biaxial xy pressure and a uniaxial pressure along the z-direction. Our calculations has been performed in the temperature range of 0 to 300 K. Fig. 7.8 shows the temperature dependence of C_{11} and C_{22} at zero pressure and at 8 kbar (800 MPa) pressure. In the ferroelastic phase, C_{11} increases by 32% in the vicinity of the transition temperature whereas C_{22} decreases by about 5.4% with cooling. However in paraelastic phase, both elastic constants decrease continuously with cooling.

Fig. 7.9 shows that the elastic constant C_{33} remains constant in the paraelastic phase. The same type of behaviour has been presented by authors in Ref. [10]. However, in the ferroelastic (monoclinic) phase C_{33} decreases by 5 % as the temperature decreases below T_c. Study of Wu [14] shows that the elastic constant C_{33} does change by 3% in the vicinity of the phase transition. According to the study of Wu [14], it has also been reported that C_{33} keeps increasing with further cooling in the monoclinic phase down to 25 K, which is a consequence of normal thermal behaviour of the corresponding acoustic phonons. Therefore, our calculations of the elastic constant show

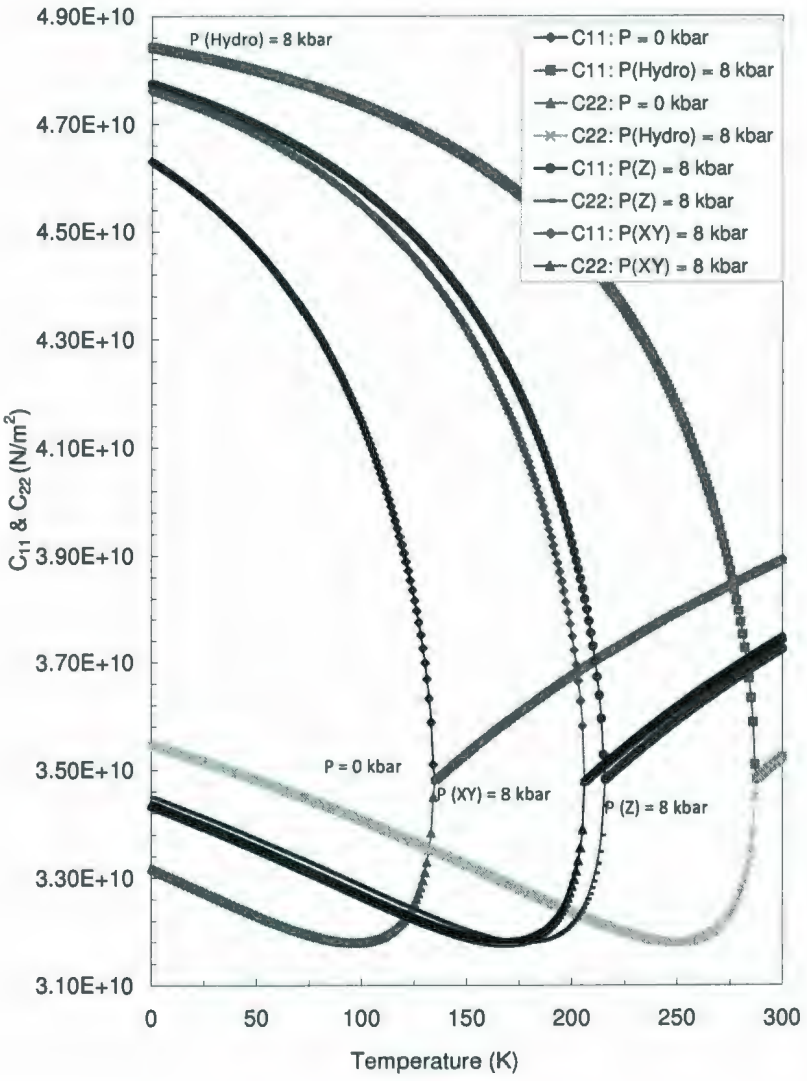

Figure 7.8: Temperature dependence of elastic constants C_{11} and C_{22} at various applied pressures.

a good agreement with the data presented by the authors in Ref. [10]. Ultrasonic study of RLHS by Breczewski et al. [10] shows that, in the temperature range 140 to 298K, the elastic constants C_{33}, C_{44}, C_{66}, C_{13}, and C_{16} are almost constant while C_{11} decreases with cooling. Thus, in agreement with our calculation the elastic constant C_{11} shows softening in the vicinity of the transition temperature.

According to the study of Wu [14] it has been pointed out that the variations in the elastic constants C_{44} and C_{66} are remarkably small with cooling. At the transition temperature C_{66} shows a very small change while C_{44} shows a slight change in slope. According to our calculation presented in Fig. 7.10, it has been observed that in the high temperature phase C_{44} is constant regardless of the pressure applied. However, in the ferroelastic phase C_{44} decreases by 1.6% below T_c. Contrary to C_{44} and C_{55}, C_{66} is pressure dependent in the tetragonal phase as shown in Fig. 7.12. Moreover, C_{66} exhibits the same phenomenological behaviour as C_{11}, with the application of any kind of stresses.

In our calculation, the elastic constant C_{12} increases by 31% between 0 K and the critical temperature. However, in the paraelastic phase it decreases with further increase in temperature. Wu [14] measured C_{12} in the tetragonal phase and reported that it decreases with temperature, consistent with our calculation. Fig. 7.14 displays the temperature dependence of the elastic constant C_{13} at various pressures. In our calculations, in tetragonal phase indicate that the elastic constant C_{13} remains constant regardless of the pressure. In the monoclinic phase the value of C_{13} decreases by 12% below T_c.

The measurement of C_{16} by Breczewski et al. [10] shows that it is constant. This is not reflected in our calculation presented in Fig. 7.15. Our calculation shows that C_{16} decreases with temperature up to T_c then it increases with further increase in temperature.

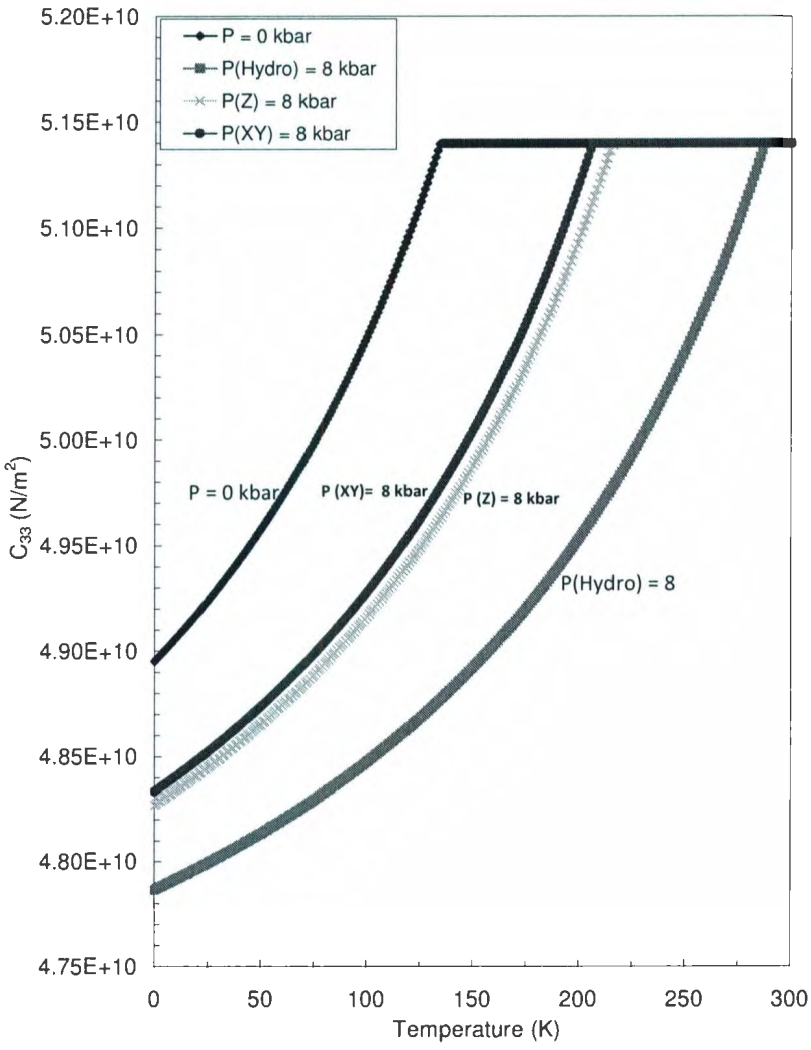

Figure 7.9: Temperature dependence of elastic constant C_{33} at various applied pressures.

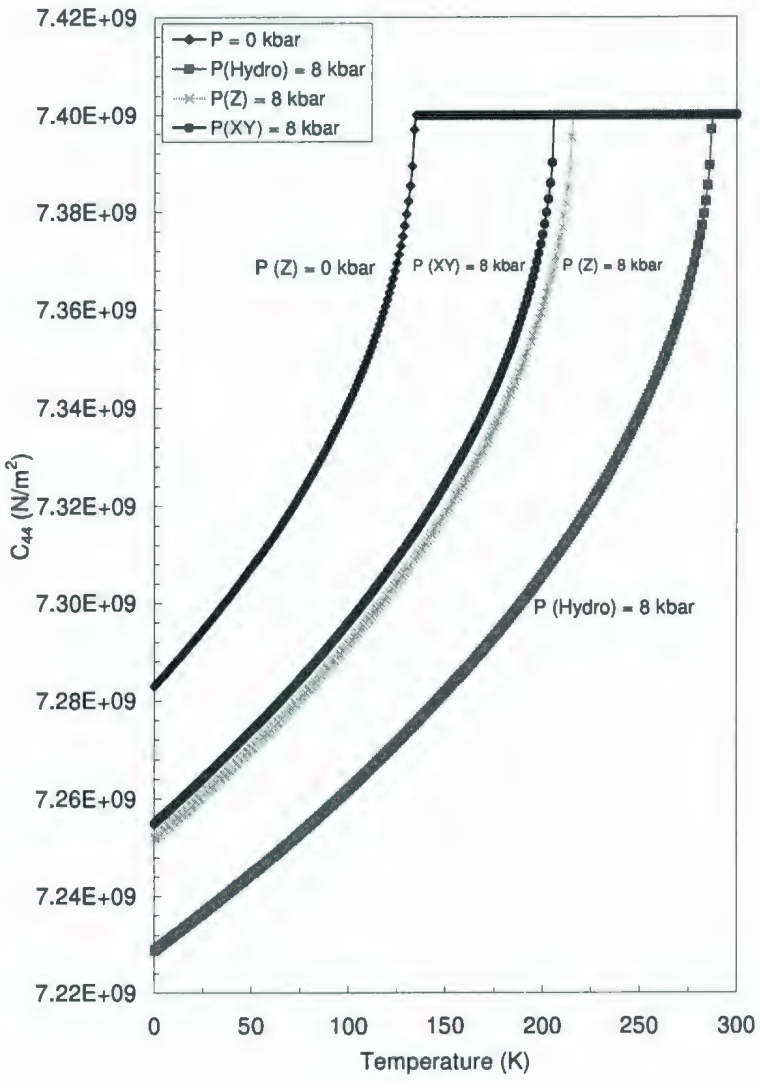

Figure 7.10: Temperature dependence of elastic constant C_{44} at various applied pressures.

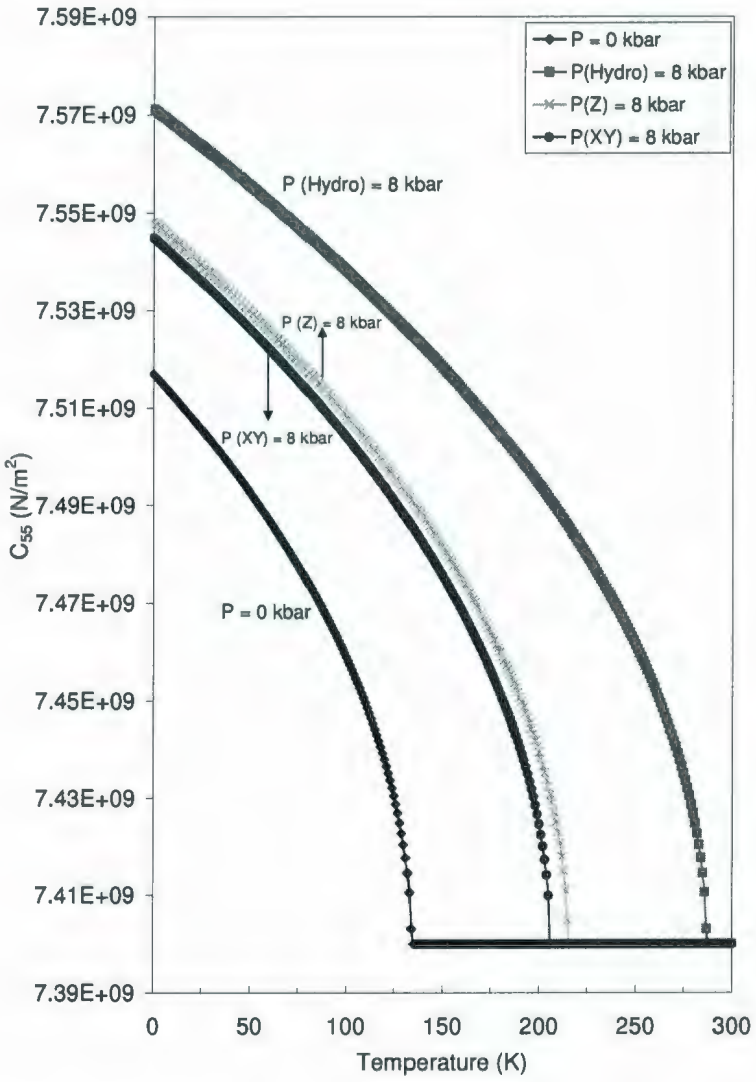

Figure 7.11: Temperature dependence of elastic constant C_{55} at various applied pressures.

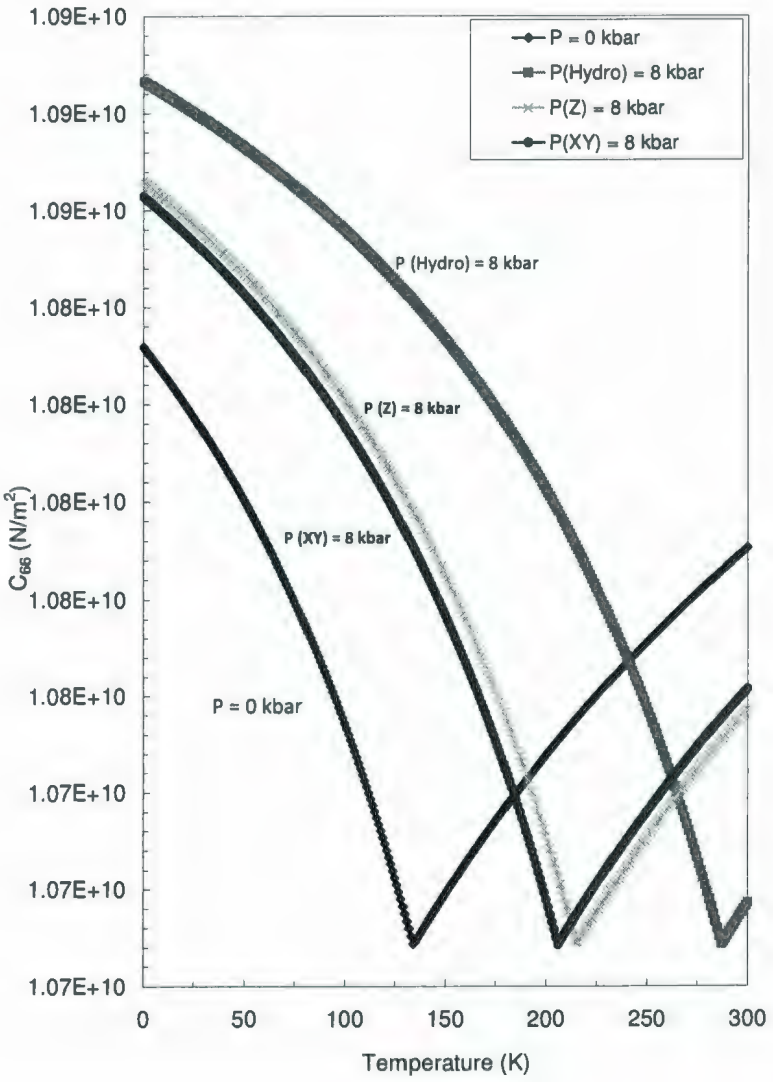

Figure 7.12: Temperature dependence of elastic constant C_{66} at various applied pressures.

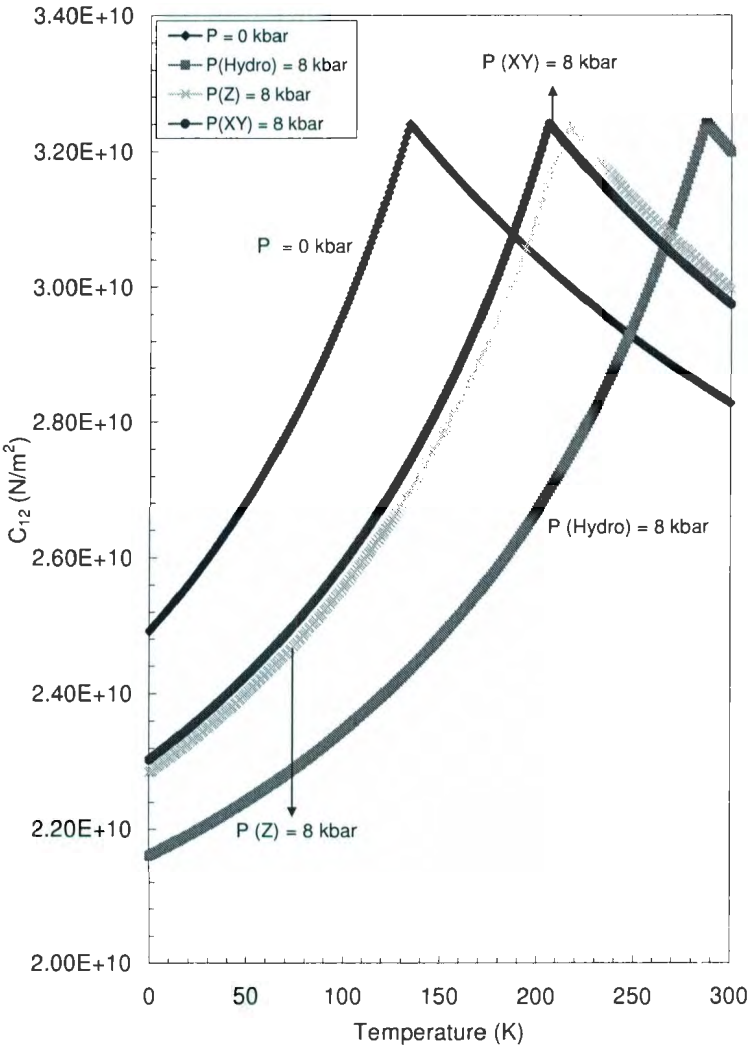

Figure 7.13: Temperature dependence of elastic constant C_{12} at various applied pressures.

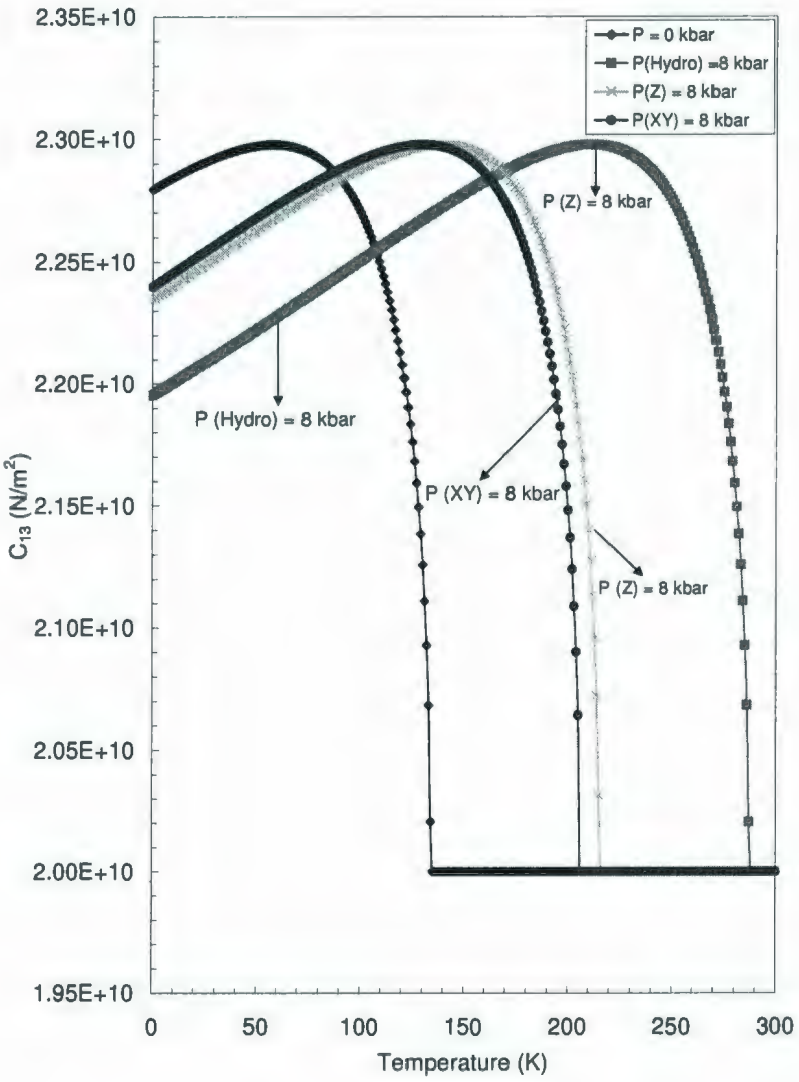

Figure 7.14: Temperature dependence of elastic constant C_{13} at various applied pressures.

The results presented in Fig. 7.18 show that the elastic constant C_{36} does not show any remarkable change with the application of any kind of pressure at 0 K. As the temperature increases it decreases continuously and at the phase transition temperature it shows a quick fall and vanishes in the tetragonal phase. In the light of Landau model, let us discuss about the elastic constant C_{45} which is displayed in Fig. 7.19. Like C_{36}, this elastic constant is zero in the tetragonal phase. However, in the ferroelastic phase it exhibits exactly the same type of characteristics with the application of different kinds of stresses as is observed in C_{11}, C_{22}, C_{55}, C_{66}, and C_{16}.

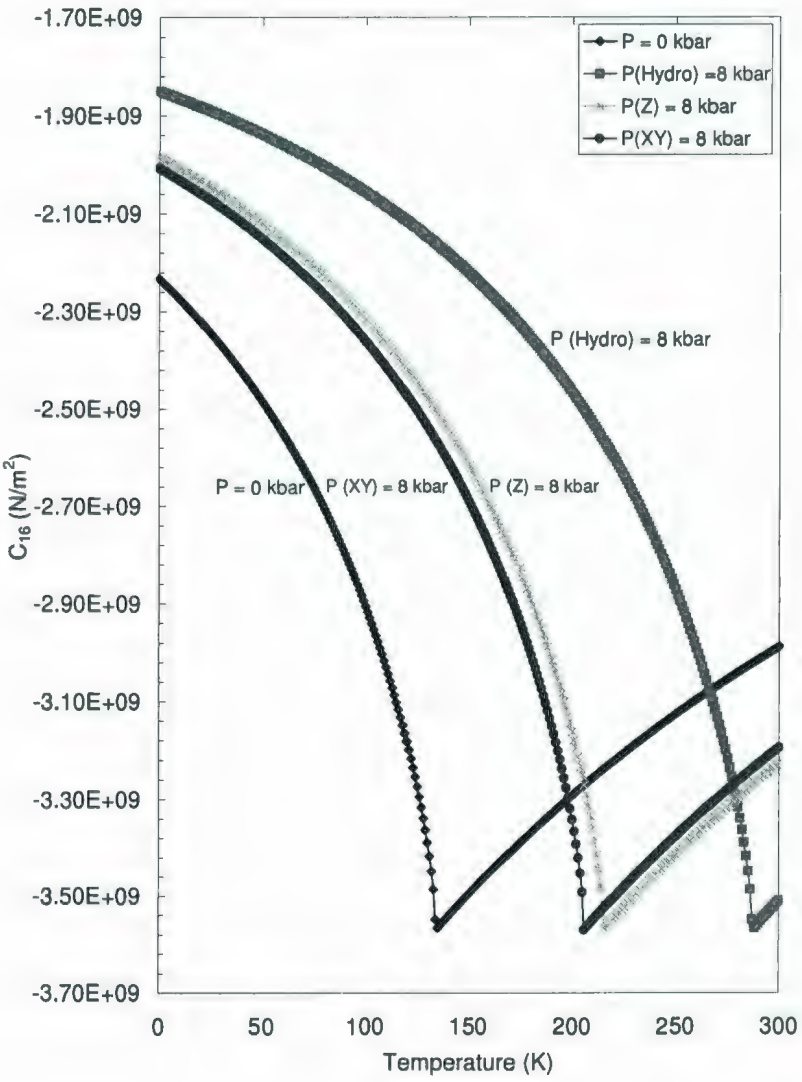

Figure 7.15: Temperature dependence of elastic constant C_{16} at various applied pressures.

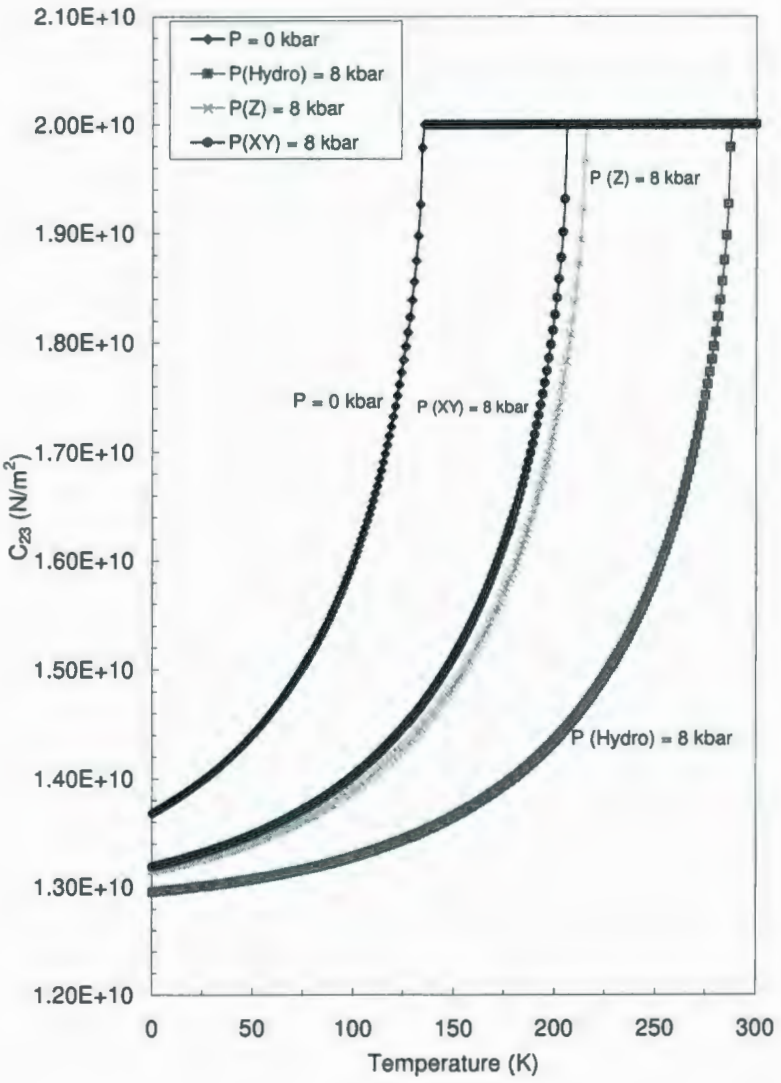

Figure 7.16: Temperature dependence of elastic constant C_{23} at various applied pressures.

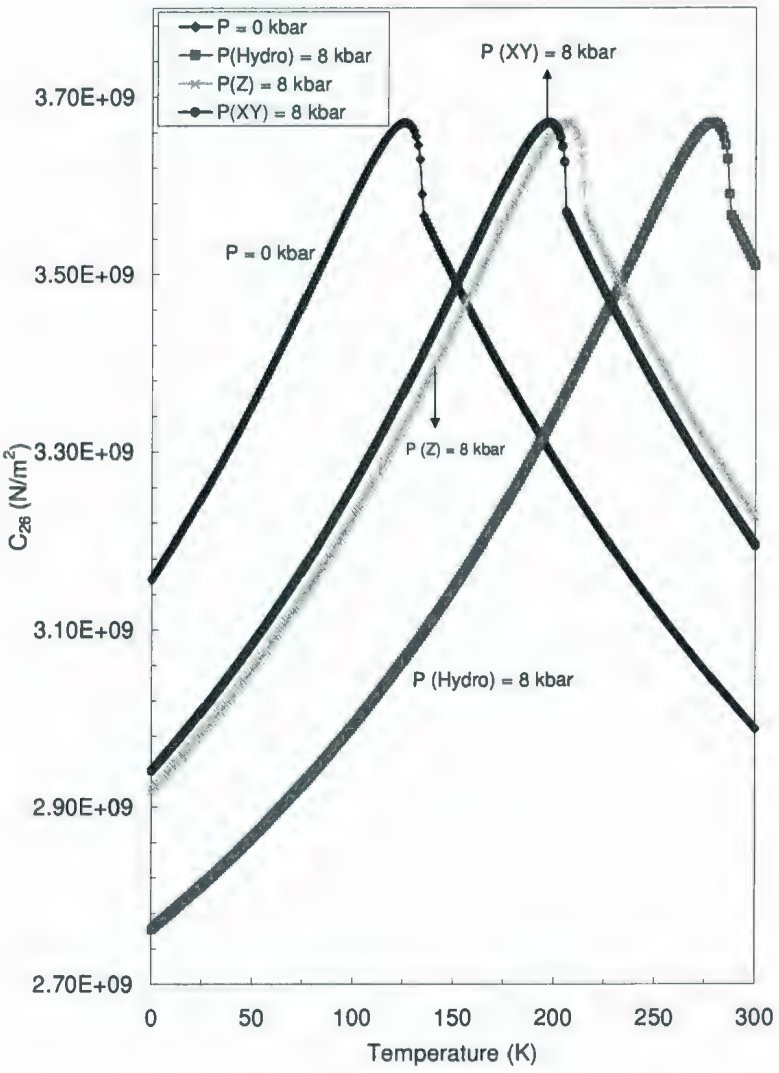

Figure 7.17: Temperature dependence of elastic constant C_{26} at various applied pressures.

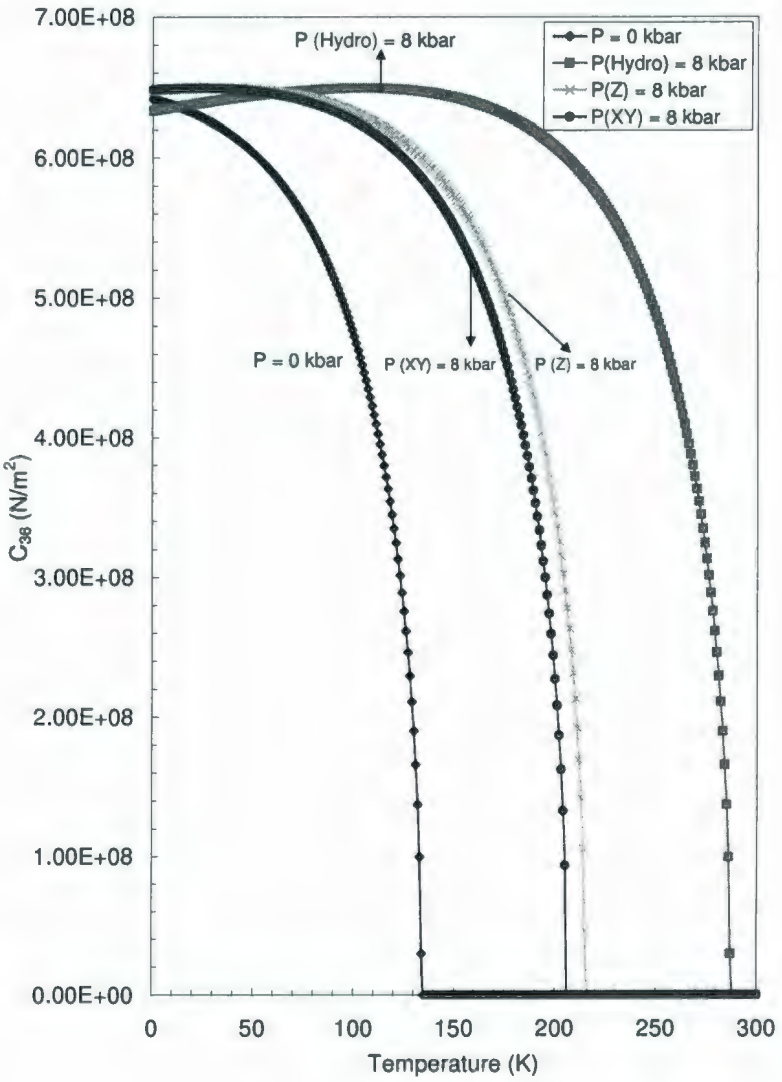

Figure 7.18: Temperature dependence of elastic constant C_{36} at various applied pressures.

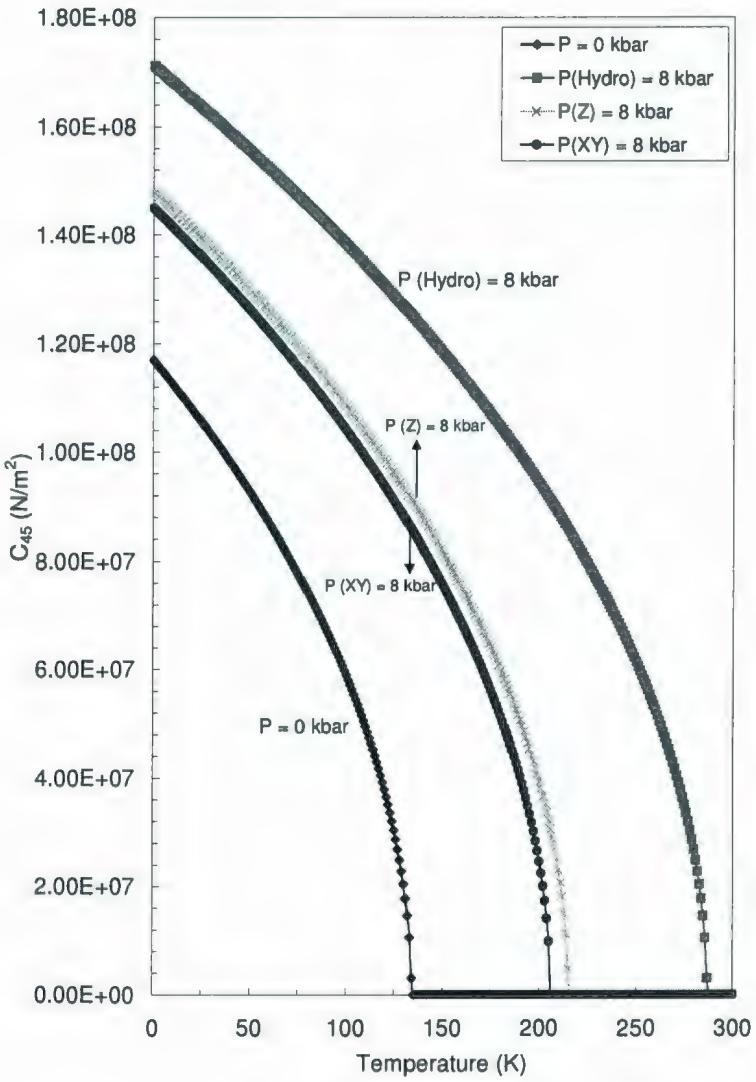

Figure 7.19: Temperature dependence of elastic constant C_{45} at various applied pressures.

Chapter 8

Results and Discussion

8.1 Sample Preparation

The $Rb_4LiH_3(SO_4)_4$ single crystal was grown by slow evaporation method from an acid aqueous solution ($P_H < 1$) in the Crystal Physics Laboratory of Adam Mickiewicz University, Poznan, Poland [7, 34]. To perform the ultrasonic measurements two samples with parallel faces perpendicular to the crystallographic axes were prepared. The samples were cut from large colorless and transparent single crystals. To get a good signal, the opposite faces of the sample were polished using aluminum oxide until they were smooth and parallel to each other. The sample dimensions were 1.42 mm × 1.63 mm × 5.56 mm and 1.95 mm × 3.21 mm × 3.13 mm. The samples orientations were also checked with polarized light. RLHS single crystals possess an optic axis along the c-axis so that the polarization of the light beam is modified after passing through the crystal. Thus, the sample orientation can be rapidly verified by putting the sample between polarizers with their transmission axes rotated by 90° with respect to each other. As the sample is rotated about its z-axis, we observe no change in the intensity of the light transmitted through the sample. Whenever the

sample is rotated about either x- or y-axis, the intensity is reduced significantly.

In this chapter we present sound velocity measurements, obtained on RLHS as a function of temperature without and with stress. Consequently, we also discuss the validity of the proposed Landau model in the ferroelastic phase.

8.2 Sound Velocity Measurements

The absolute velocity of longitudinal waves propagating along [001] and perpendicular to this direction have been performed using the transmission configuration. If Δt is the time of flight for a sample of length L, then the absolute sound velocity is calculated using,

$$v = \frac{L}{\Delta t} \quad . \tag{8.1}$$

To obtain a better estimate of the absolute sound velocity we have considered the first four echoes. The corresponding time of flights have been measured from an oscilloscope. As shown in Fig. 8.1, the distance travelled as a function of the time of flight is essentially a straight line. The slope gives an average value of the absolute sound velocity. Our measurement of the velocity of longitudinal waves propagating along [001], $v_3 = 3430 \pm 30$ m/s, agrees well with that reported by Wu [14] and Breczewski et al. [10].

8.3 Comparison of the Model and Experimental Data

The elastic constants of any material can be determined using sound velocity measurements. As long as the crystal structure is known, the relationship between the

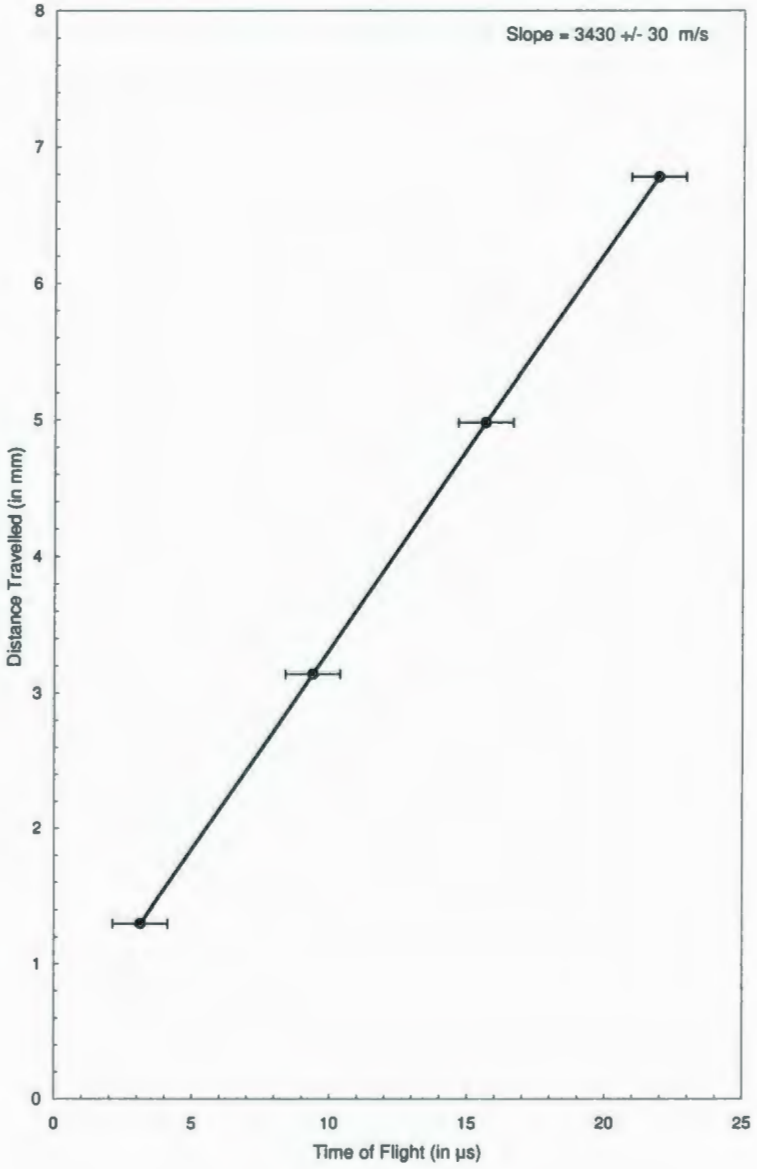

Figure 8.1: Absolute sound velocity of longitudinal waves propagating along [001] direction in RLHS.

sound velocity and the elastic constants for any particular acoustic mode can be calculated using Christoffel's equation (See Eq. 4.43). Generally, the sound velocity and the elastic constants are related via the relation

$$v = \sqrt{\frac{C_{eff}}{\rho}} \quad . \tag{8.2}$$

The experimental results are then compared to predictions derived from the Landau free energy. The goal of this project is to test the validity of the Landau model in the monoclinic phase. In earlier measurements, it was reported [14] that the theoretical model agrees well with results obtained in the tetragonal phase, while the agreement with data obtained in the monoclinic phase is not so good. It has been suggested that this is due to the fact that there are structural domains in the monoclinic phase. In order to remove these domains, we applied a uniaxial stress along [100] or [010] while we measure the sound velocity of longitudinal waves propagating along the [001] direction.

In this section, we analyze the data obtained using longitudinal waves propagating along the [001] direction. From these measurements, we obtain v_3 related to the elastic constant C_{33} via the relation $v_3 = \sqrt{\frac{C_{33}}{\rho}}$. Tylczynski et al. [49] studied the influence of uniaxial stress on v_3 in the ferroelastic compound $NH_4LiH_3(SO_4)_4$. As this compound shows a $4 \rightarrow 2$ ferroelastic transition identical to that observed in RLHS, results obtained on this isomorphic compound can be used for comparison. According to their measurements, in the absence of stress, v_3 undergoes a typical step-like change of about 1% around the critical temperature (see Fig. 8.2). Afterwards, as the stress is applied along the xy-plane the step amplitude decreases with increasing stress, until it disappears completely above the coercive stress. The authors attribute this variation to a typical pressure dependence. However, we rather believe that this is due to the fact that the stress gradually transforms the sample into a single domain.

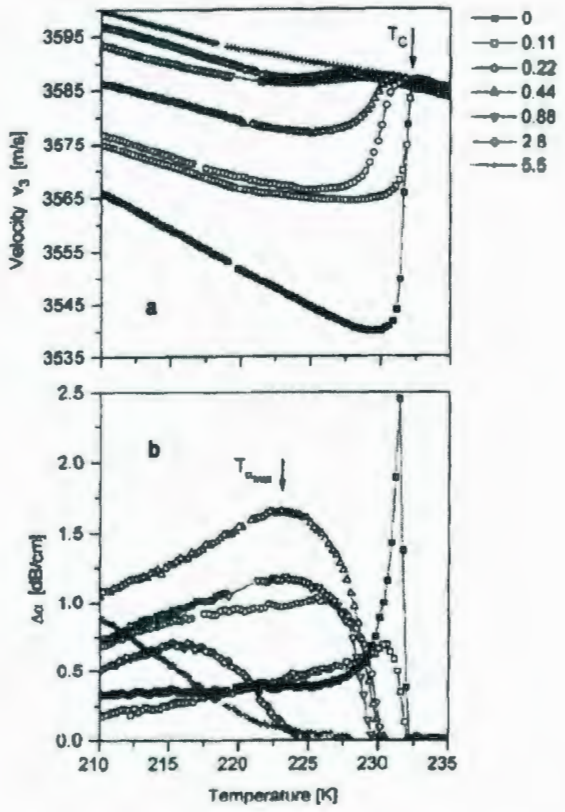

Figure 8.2: Velocity of the longitudinal wave propagating in $NH_4LiH_3(SO_4)_4$ along [001] direction for different stress applied (in MPa). Data extracted from Tylczynski et al. [49].

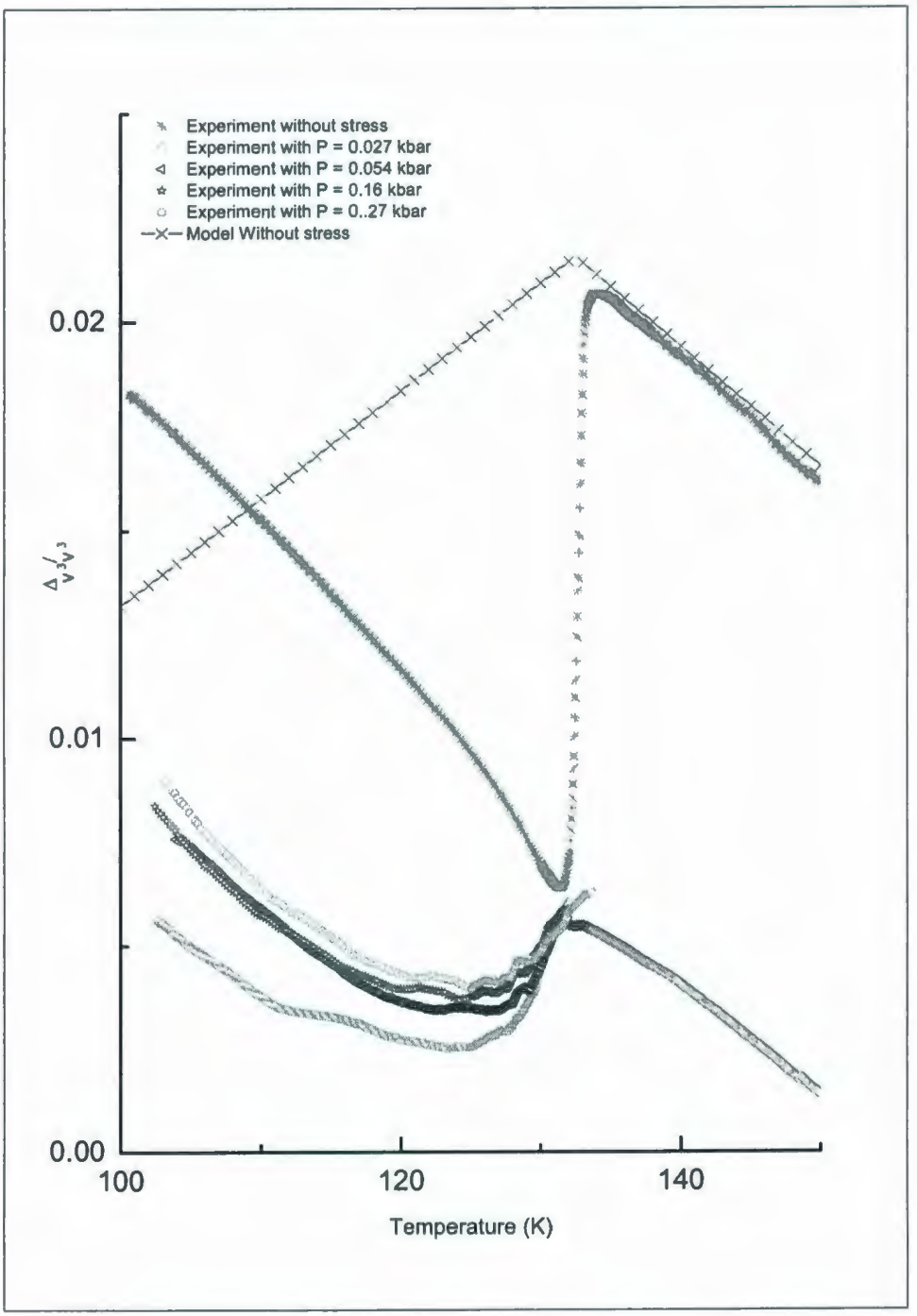

Figure 8.3: Longitudinal waves propagating in $Rb_4LiH_3(SO_4)_4$ along [001] direction with and without stress applied (in kbar).

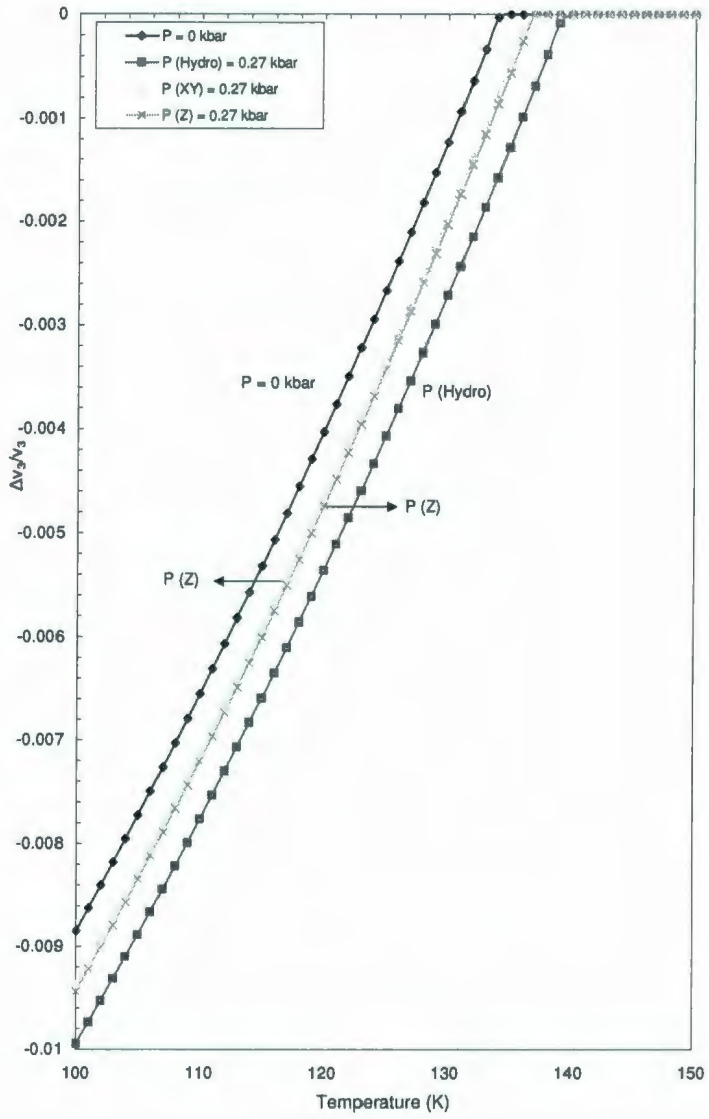

Figure 8.4: Plot of $\frac{\Delta\upsilon_3}{\upsilon_3}$ as function of temperature without stress and with a stress (hydrostatic stress, stress along xy-plane and a uniaxial stress) of 0.27 kbar (27 MPa), obtained from our theoretical predictions.

Our experimental data and model for the longitudinal waves propagating along [001], with and without stress are presented in Fig. 8.3. Here the stress is applied either along [100] or [010]. According to the experimental data presented in Fig. 8.3, the sound velocity v_3 changes by 1.5 % while this change is reduced to 0.5 % with a uniaxial stress of 0.27 kbar (27 MPa). The general trend with increasing pressure is similar to the one shown in Fig. 8.2 in the case of $NH_4LiH_3(SO_4)_4$.

The comparison between the experimental data and pseudoproper model is also shown in Fig. 8.3. Experimental results are presented by the symbols while solid line with cross marks represents the prediction of the model. If we compare the experimental data of v_3 without stress with that of the model, it is found that the model does not agree well with the experimental data in the tetragonal phase. In order to make the model consistent with the experimental data in the tetragonal phase [12] we have added a linear function in the tetragonal phase of the model. The difference between the experimental data and the model prediction below the phase transition might be associated with the presence of ferroelastic domains [12]. This is somehow surprising as the domains are oriented normal to the z-direction. However, the experimental data as a function of pressure also show that ferroelastic domains have a large effect on the velocity of acoustic waves propagating along the z-direction. With a small pressure of 0.27 kbar we observe a decrease of 60 % in the velocity variation at T_c. This variation can be compared to the model prediction shown in Fig. 8.4. In all cases, the predictions show an increase of about 10 % for a pressure of 0.27 kbar. The model also predicts a change in T_c from 134 K to 137 K with a pressure of 0.27 kbar (27 MPa) applied in the xy-plane. However, no significant variation in the value of T_c has been observed experimentally. This might be attributed to the fact that the actual pressures are much smaller than those estimated. As domains are ignored in the theoretical model, we thus believe that the observed variation in

the step amplitude is due a change into the domain configuration.

8.4 Stress Applied Along [100] or [010]-direction

In this section we present the experimental data of ultrasonic measurements realized on RLHS using longitudinal waves propagating along [100] with and without a stress applied along the [010] direction. All measurements were done in the temperature range of 100 to 150 K. Fig. 8.5 shows the experimental data and model for the sound velocity v_2 with and without stress. The broken lines with squares and circles represent the experimental data while the solid line with cross marks represents the prediction of the theoretical model. The maximum stress applied was 0.13 kbar (13 MPa). Measurements without stress has been done by keeping a clear gap between the actuator and the sample. According to the experimental data presented in Fig. 8.5, without the application a stress, the sound velocity v_2 shows a step-like variation of 3.3 % at the phase transition. This compares well with ultrasonic study realized by Quirion et al. [12]. Comparing the experimental data without stress with the model without stress, we find that our pseudoproper model agrees well with experiment around the phase transition. Below the phase transition until 123 K, the trend of the model and experiment is of similar type. However, with further cooling below 123 K the experimental data of v_2 increases linearly with further cooling while the model shows a continuous decrease with further cooling. As we apply a stress of 0.13 kbar (13 MPa) along the [100] direction, the phase transition is barely noticeable. After removing the stress, the signal did not improve. This might be attributed to a serious degradation of the mechanical bonding between the sample and the transducers. Thus, for that mode no reliable data under pressure has been obtained.

Fig. 8.6 presents the numerical predictions of our theoretical model. As the pres-

sure is applied in the tetragonal phase, the sound velocity v_2 decreases with pressure. In the tetragonal phase, we also find the sound velocity v_2 decreases linearly with cooling. However, below the phase transition, v_2 shows a change of about 0.5 % down to 105 K and below. Below 105 K, all curves with or without stress overlap indicating that no large variation in the sound velocity v_2 should be observed as a function of temperature in the monoclinic phase with stress. Unfortunately, as mentioned previously, we were unable to obtain experimental data for that mode.

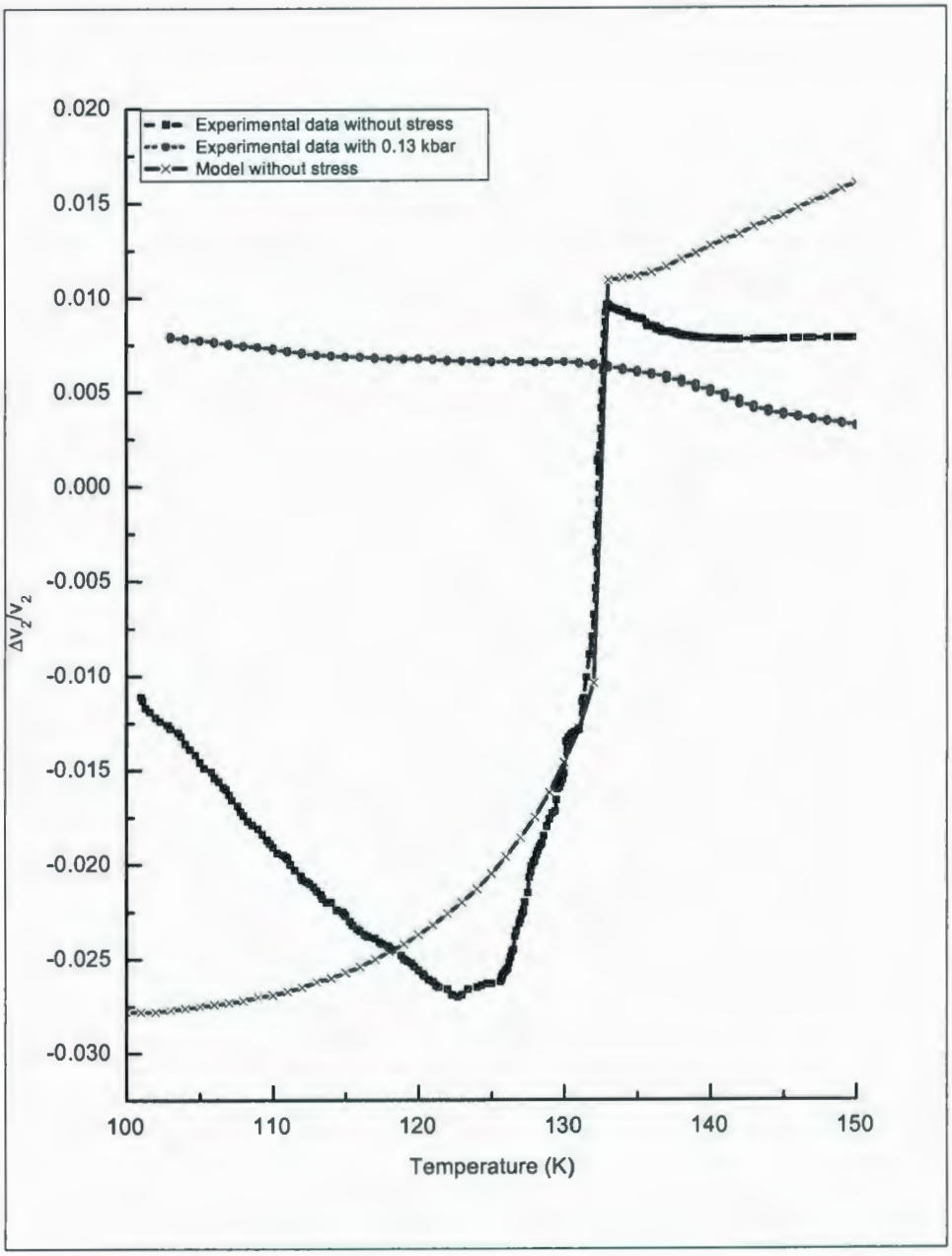

Figure 8.5: Ultrasonic data of RLHS with and without stress. Stress is applied along [100] or [010] direction and measurements are performed perpendicular to that direction. The amount of stress applied is 0.13 kbar (13 MPa).

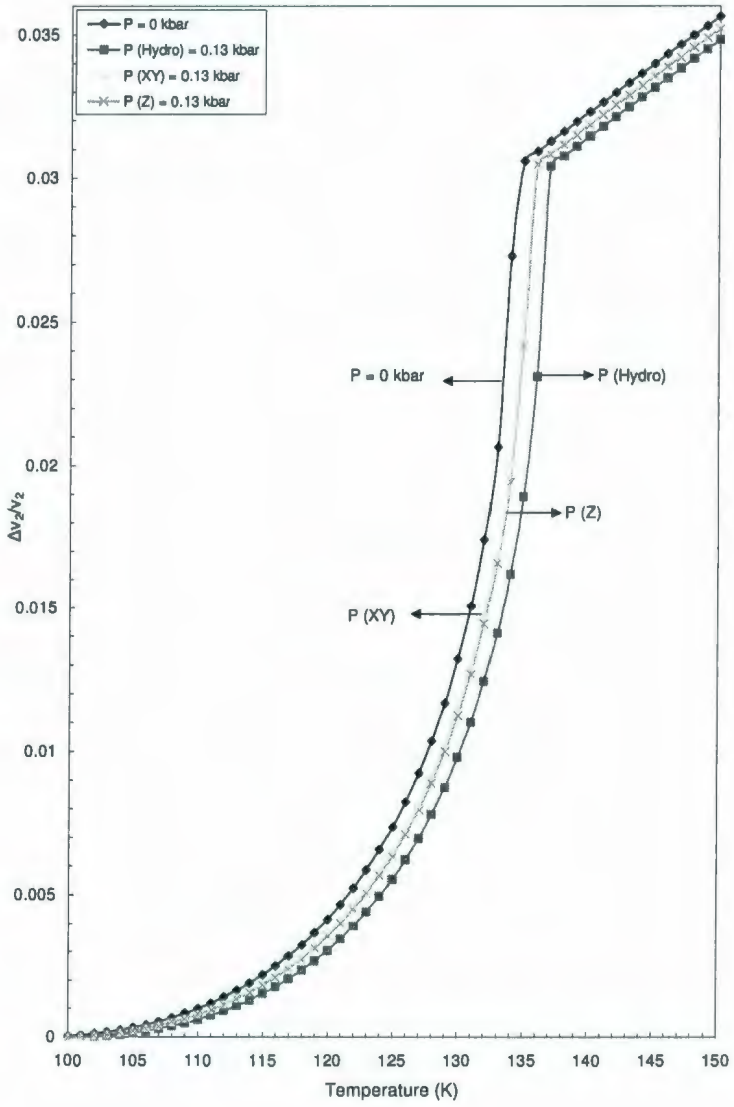

Figure 8.6: Plot of $\frac{\Delta v_2}{v_2}$ as function of temperature without stress and with a stress (hydrostatic stress, stress along xy-plane and a uniaxial stress) of 0.13 kbar (13 MPa), obtained from our theoretical predictions.

Chapter 9

Conclusions

Even though the elastic properties of RLHS have been studied by different authors [10, 12, 14], still there are controversy regarding the driving mechanism of the phase transition. As the point groups satisfy the group-subgroup relation, a Landau model has been used to explain the observed phase transition. As mentioned in Chapter 2, a number of Landau models have been proposed by various groups [5, 7, 9, 10, 12, 13, 14, 50]. Among them, one group considers that the driving mechanism for the transition is the spontaneous strain. This type of transition is called a proper ferroelastic transition [5, 7, 9]. Other groups assume that the order parameter is a physical quantity other than the strains; the transition is referred as pseudoproper ferroelastic [10, 12, 13, 14]. Recent ultrasonic study by Quirion et al. [12] and Raman scattering investigation by Oktay et al. [48] confirmed that the phase transition observed at $T_c = 134$ K in RLHS is a pseudoproper transition driven by the softening of a B symmetry optic mode. Therefore, in our study the experimental data of elastic constants of RLHS have been analyzed within the framework of the pseudoproper Landau model. The proposed models have been also used to determine the temperature dependence of the order parameter at different pressures, the pressure dependence of the spontaneous strains,

and the pressure dependence of the transition temperature. According to the Landau analysis for various stresses we obtained that the transition temperature shows the largest increase for a hydrostatic pressure of 8 kbar while the smallest variation is produced by a uniform pressure applied in the xy-plane. This is consistent with the study of pressure dependence of the strains at 300 K which shows that the critical pressure of RLHS is 18.4 kbar (1.84 GPa) for a pressure applied in xy-plane, whereas the critical pressure P_c is 8 kbar (800 MPa) for a hydrostatic pressure.

In this work, the effect of a uniaxial pressure on the elastic properties of RLHS has been performed using a high resolution acoustic interferometer device. Moreover, the data have been analysed using a phenomenological Landau model. In our experimental work, the ranges of temperature and pressure are 100 to 150 K and 0 to 0.27 kbar (27 MPa), respectively. However, for the theoretical calculations the temperature and pressure ranges have been extended to 0 to 300 K and 0 to 8 kbar (800 MPa), respectively. Ultrasonic measurements show that at ambient pressure RLHS undergoes a structural phase transition at $T_c = 134$ K, showing no thermal hysteresis on successive heating and cooling processes. This confirms that the phase transition is second order. Using the transmission configuration, the absolute sound velocity of RLHS has been measured. Our results agree with the ultrasonic data obtained by other groups [12, 14].

The low and high temperature phases of RLHS are monoclinic and tetragonal, respectively. Our ultrasonic measurements as a function of temperature reveal that the the variation in the sound velocity v_3 around T_c is significantly reduced with the application of a uniaxial pressure applied along the x-axis. With a uniaxial stress of 0.27 kbar (27 MPa) along [100] or [010], direction the change in v_3 is reduced to 0.5 % at the phase transition. In this case, the measurements have been done along [001] direction of the crystal. This might indicate that domains in the monoclinic phase of

RLHS disappear with the application of a uniaxial stress along [100] direction. This change in the domain configuration leads to a reduction in the sound velocity v_3 at the vicinity of the phase transition.

The temperature dependences of the 13 independent elastic constants of RLHS have been analyzed in the light of the pseudoproper Landau model at zero and 8 kbar pressure. According to our analytical predictions of the propsed model, the magnitudes of the elastic constants C_{11}, C_{22}, C_{55}, C_{66}, C_{16}, and C_{45} increase with the application of stresses. However, the magnitudes of the elastic constants C_{33}, C_{44}, C_{12}, C_{13}, C_{23} and C_{26} decrease with the application of stresses at 0 K. The temperature behaviour of the elastic constant C_{11} was found to agree well with the study by Wu [14] in both phases while C_{33} shows a good agreement with Ref. [10]. The study of Wu [14] reported that in tetragonal phase C_{12} increases linearly with cooling, consistent with our analysis. Due to the lack of data for the elastic constants C_{55}, C_{23}, C_{26}, C_{36}, and C_{45} we could not present comparison with our numerical predictions.

It has been clearly demonstrated by earlier studies [14] that a pseudoproper Landau model quantitatively describes the temperature and pressure dependence of the elastic constants in the tetragonal phase of RLHS. Deviations in the monoclinic phase was attributed to ferroelastic domains which appear in that phase. This is supported by our measurements under a uniaxial stress applied along [100]. The observed variation at T_c is ten times larger than our numerical predictions which ignore the presence of domains. In our experiments, uniaxial pressures were applied either along [100] or [010]-direction and measurements were done along [001] and [010]-directions. Unfortunately, we were not able to solve the Landau free energy in this case. However, we were able to manage the Landau free energy for three other stresses (hydrostatic stress, biaxial stress along xy-plane and a uniaxial stress along z-direction). Thus,

we belive that the solution for a uniaxial stress along [100] or [010] similar to results presented in Fig. 8.4 and Fig. 8.6. According to the Fig. 8.4, with the application of hydrostatic, biaxial or a uniaxial stress, the sound velocity v_3 shows an increase in the amplitude of the variation at T_c while the experiment shows the opposite trend (see Fig. 8.3).

Bibliography

[1] G. Varughese, A. S. Kumar, A. V. Alex, J. Philip, and L. Godfrey, *Ferroelectrics,* ***323,*** 133 (2005).

[2] M. Polomska, and F. Smunty, *Phys. Status Solidi b,* ***154,*** K103 (1988).

[3] J. Minge, and T. Krajewski, *Phys. Status Solidi a,* ***109,*** 193 (1988).

[4] T. Wolejko, G. Pakulski, and Z. Tylczynski, *Ferroelectrics,* ***81,*** 1979 (1989).

[5] P. Piskunowicz, T. Breczewski and T. Welejko, *J. Phys. Stat. Sol. (a)****114,*** 505 (1989).

[6] T. Krajeski, T. Breczewski, P. Piskunowicz, and B. Mroz, *Proc. 8th Czechoslovak-Polish Seminar on Structural and Ferroelastic Phase Transitions, Senohraby,* (1988).

[7] B. Mróz, H. Kiefte, M. J. Clouter, and J. A. Tuszynski, *J. Phys. Condens. Matter,* ***3,*** 5673 (1991).

[8] B. Mróz, M. Kraczmarski, H. Kiefte, M. J. Clouter, *J. Phys. Condens. Matter,* ***4,*** 7515 (1992).

[9] H. Hempel, H. Maack and G. Sorge, *Phys. Stat. Sol. (a),* **110**, 459 (1988).

[10] T. Breczewski, A. Gomez-Cuevas, J. M. Perez-Mato, and E. H. Bocanegra, *Solid State Comm.,* ***76,*** No. 5, 639 (1990).

[11] B. Mróz, and R. Laiho, *Phys. Status Solidi, a,* ***115,*** 575 (1989).

[12] G. Quirion, W. Wu and J. Rideout, *Landau Model for the Ealstic Properties of the Ferroelastic Crystal* $Rb_4LiH_3(SO_4)_4$, available at http://arxiv.org/PS$_{cache}$/*condmat*/*pdf*/0606/0606064*v*1.*pdf*.(2006).

[13] O. Aktas, *Raman Spectra of the B Mode of the Ferroelastic Compound* $Rb_4LiH_3(SO_4)_4$ *as a Function of Temperature,* M. Sc Thesis, Dept. of Physics & Physical Oceanography, Memorial University, St. John's, NL, A1B 3X7 (2008).

[14] W. Wu, *Investigation of the Elastic Properties of* $Rb_4LiH_3(SO_4)_4$ *as a Function of Temperature and Pressure,* M. Sc Thesis, Dept. of Physics & Physical Oceanography, Memorial University, St. John's, NL, A1B 3X7 (2004).

[15] K. H. Stewart, *Ferromagnetic Domains,* Methuen / Co. Ltd., London (1969).

[16] Nicola Spaldin, *Magnetic Materials: Fundamentals and Device Applications,* Cambridge University Press, Cambridge (2003).

[17] V. K. Wadhwan, *Bull. Mater. Sci.,* ***6,*** 733 (1984).

[18] M. Guymont, *Phase Transitions,* ***34,*** 135 (1991).

[19] V. K. Wadhawan, *Phase Transitions,* ***34,*** 3 (1991).

[20] E. K. H. Salje, *Phys. Rep.,* ***55,*** 37 (1992).

[21] A. Aird and E. K. H. Sajle, *J. Phys.: Condens. Matter,* ***10,*** L 377 (1998).

[22] M. A. Carpenter and E. K. H Sajle, *Eur. J. Mineral.,* ***10,*** 693 (1998).

[23] J. Fousak, D. B. Litvin and L. E. Cross, *J. Phys.: Condens. Matter,* ***13,*** L33-L38 (2001).

[24] E. K. H. Salje, *Contemporary Physics,* ***41,*** 2, 79-91 (2000).

[25] P. Toledano, M. M. Fejer, and B. A. Auld, *Phys. Rev. B,* ***27,*** 5717 (1983).

[26] W. Rehwald, *Adv. Phys.,* ***22,*** 721 (1973).

[27] R. A. Cowley, *Phys. Rev. B,* ***13,*** 4873 (1976).

[28] G. Errandonea, *Phys. Rev. B,* ***21,*** 5221 (1980).

[29] F. Schwabl, *Ferroelectrics,* ***24,*** 171 (1980).

[30] J. -C. Toledano, G. Errandonea and J. P. Jaguin, *Solid State Commun.,* ***20,*** 905 (1976).

[31] W. I. F. David and I. G. Wood, *J. Phys. C: Solid State Phys.,* ***16,*** 5149 (1983).

[32] A. Bulou, M. Rousseau and J. Nouet, *Key Engg. Mater.,* ***68,*** 133 (1992).

[33] L. H. Brixner, J. F. Whitney, F. C. Zumsteg and G. A. Jones, *Mater. Res. Bull.,* ***12,*** 17 (1977).

[34] G. Nalini, and T. N. G. Row, *Proc. Indian Acad. Sci. (Chem. Sci.),* ***115,*** Nos. 5 6, 473 (October-December 2003).

[35] F. J. ZúŤildeniga, J. Etxebarria, G. Madariaga and T. Breczewski, *Acta Cryst. C,* ***46,*** 1199 (1990).

[36] B. Mróz, S. M. Kim, B. M. Powell et al., *Phys. Rev. B,* ***55,*** 11174 (1997).

[37] K. Aizu, *J. Phys. Soc. Jpn.,* ***27,*** 387 (1969).

[38] C. Boulesterix, *Phys. Stat. Sol. A),* ***86,*** 11 (1984).

[39] E. K. H. Saljee, *Phase Transitions in Ferroelastic and Co-elastic Crystals,* Cambridge University Press (1993).

[40] L. D. Landau and E. M. Lifshitz, *Theory of Elasticity,* Second Edition, Pergamon Press, Addison-Wesley Publishing Company, Inc. Massachusetts (1970).

[41] E. Dieulesaint and D. Royer, *Elastic Waves in Solids: Applications to Signal Processing,* John Wiley and Sons Ltd. (1980).

[42] G. Quirion, M. Abu-Kharama, I. A. Sergienko, M. Bromberek, M. J. Clouter and B. Mróz, *J. Phys. Condens. Matter* ***15,*** 4979 (2003).

[43] C. N. Rao and K. J. Rao, *Phase Transitions in Solids,* McGraw-Hill, New York (1978).

[44] V. K. Wadhawan, *Introduction to Ferroic Materials,* Gordon and Breach Science Publishers, (2000).

[45] P. Papon, J. Leblond and P. H. E. Meijer, *The Physics of Phase Transitions: Concepts and Applications,* Springer, Heidelberg (2002).

[46] J. Toledano and P. Toledano, *The Landau Theory of Phase Tansitions,* World Scientific, New Joursey (1987).

[47] V. L. Gingburg and L. D. Lnadau, *Collected Papers of L. D. Landau,* Edited by D. Ter. Haar Pergamon Press, Oxford (1965).

[48] O. Aktas, M. Clouter and G. Quirion, *J. Phys.: Condens. Matter,* ***21,*** 285901 (2009).

[49] Z. Tylczynski and B. Mroz, *Solid State Commun.* ***111,*** 9, 653 (1997).

[50] B. Mróz, J. A. Tyszynski, H. Kiefte, and M. J. Clouter, *J. Phys.: Condens. Matter,* ***1,*** 4425 (1989).